

OPEN ACCESS

Long-Term Stability of Ferri-/Ferrocyanide as an Electroactive Component for Redox Flow Battery Applications: On the Origin of Apparent Capacity Fade

To cite this article: Eric M. Fell *et al* 2023 *J. Electrochem. Soc.* **170** 070525

View the [article online](#) for updates and enhancements.

You may also like

- [Tunable Electrochemical Grafting of Diazonium for Highly Sensitive Impedimetric DNA Sensor](#)
Su Jin Kang, Suseong Kim, Kyuhong Lee et al.
- [Long-Term Stability of Ferri/Ferrocyanide As an Electroactive Component for Redox Flow Battery Applications: On the Origin of Apparent Capacity Fade](#)
Eric M. Fell, Diana De Porcellinis, Yan Jing et al.
- [Spectroelectrochemical Examination of the Ferro-Ferricyanide Redox Reaction: Impacts of Electrode Thickness and Applied Potential](#)
Akash Ganesan, Tawanda J. Zimudzi, Vineeth Pothanamkandathil et al.



244th ECS Meeting

Gothenburg, Sweden • Oct 8 – 12, 2023

Early registration pricing ends
September 11

Register and join us in advancing science!

[Learn More & Register Now!](#)





Long-Term Stability of Ferri-/Ferrocyanide as an Electroactive Component for Redox Flow Battery Applications: On the Origin of Apparent Capacity Fade

Eric M. Fell,^{1,*} Diana De Porcellinis,¹ Yan Jing,² Valeria Gutierrez-Venegas,³ Thomas Y. George,^{1,*} Roy G. Gordon,² Sergio Granados-Focil,³ and Michael J. Aziz^{1,**,z}

¹Harvard John A. Paulson School of Engineering and Applied Sciences, 29 Oxford Street, Cambridge, MA, 02138, United States of America

²Department of Chemistry and Chemical Biology, Harvard University, 12 Oxford Street, Cambridge, MA, 02138, United States of America

³Gustaf Carlson School of Chemistry and Biochemistry, Clark University, Worcester, MA, 01610-1477, United States of America

We assess the suitability of potassium ferri-/ferrocyanide as an electroactive species for long-term utilization in aqueous organic redox flow batteries. A series of electrochemical and chemical characterization experiments was performed to distinguish between structural decomposition and apparent capacity fade of ferri-/ferrocyanide solutions used in the capacity-limiting side of a flow battery. Our results indicate that, in contrast with previous reports, no structural decomposition of ferri-/ferrocyanide occurs at tested pH values as high as 14 in the dark or in diffuse indoor light. Instead, an apparent capacity fade takes place due to a chemical reduction of ferricyanide to ferrocyanide, via chemical oxygen evolution reaction. We find that this parasitic process can be further exacerbated by carbon electrodes, with apparent capacity fade rates at pH 14 increasing with an increased ratio of carbon electrode surface area to ferrocyanide in solution. Based on these results, we report a set of operating conditions that enables the long-duration cycling of alkaline ferri-/ferrocyanide electrolytes and demonstrate how apparent capacity fade rates can be engineered by the initial system setup. If protected from direct exposure to light, the structural stability of ferri-/ferrocyanide anions allows for their practical deployment as electroactive species in long duration energy storage applications.

© 2023 The Author(s). Published on behalf of The Electrochemical Society by IOP Publishing Limited. This is an open access article distributed under the terms of the Creative Commons Attribution Non-Commercial No Derivatives 4.0 License (CC BY-NC-ND, <http://creativecommons.org/licenses/by-nc-nd/4.0/>), which permits non-commercial reuse, distribution, and reproduction in any medium, provided the original work is not changed in any way and is properly cited. For permission for commercial reuse, please email: permissions@iopublishing.org. [DOI: [10.1149/1945-7111/ace936](https://doi.org/10.1149/1945-7111/ace936)]



Manuscript submitted January 4, 2023; revised manuscript received March 13, 2023. Published July 28, 2023. *This paper is part of the JES Focus Issue on Frontiers of Chemical/Molecular Engineering in Electrochemical Energy Technologies in Honor of Robert Savinell.*

Supplementary material for this article is available [online](#)

As the global demand for sustainable electric power generation increases, aqueous organic redox flow batteries (AORFBs) offer a potential solution to the intermittency of solar and wind resources. The non-flammable electrolytes used in AORFBs contain redox-active species synthesized from Earth-abundant elements. Following the initial introduction of redox-active organics in the negolyte (negative electrolyte) of an aqueous flow battery,¹ many promising redox-active molecules have been developed as candidates for acidic, alkaline, and neutral environments.^{2–17} In contrast, very few redox-active molecules have been demonstrated as promising species for the posolyte (positive electrolyte),^{3,18–26} especially where stability is concerned. Long-term stability of redox-active molecules,^{13,27} or the ability to recompose degraded molecules,^{11,28} is a critical feature required for practical utility in a battery.

The prevalent candidate for the posolyte in an alkaline environment continues to be ferri-/ferrocyanide, $\text{Fe}(\text{CN})_6^{3-}/\text{Fe}(\text{CN})_6^{4-}$. The ferri-/ferrocyanide anion has been studied since 1839.²⁹ It has long been known that exposing neutral or alkaline pH solutions of ferrocyanide to light of wavelengths less than ~ 500 nm leads to chemical degradation of the anion to pentacyanide/iron hydroxides, whereas aqueous solutions of ferrocyanide kept in the dark, or in diffuse indoor light, are chemically stable.^{30–32} In acidic conditions, ferri-/ferrocyanide is well known to release free cyanide into solution, generating hydrogen cyanide (HCN). In early work on zinc-ferrocyanide hybrid RFBs, Adams et al. reported that ferri-/ferrocyanide is chemically stable in up to 7 N NaOH at temperatures as high as 50 °C, but above that, ferricyanide began to decompose

into electrochemically inactive iron pentacyanide, and further into insoluble iron hydroxides.¹⁸ They also hypothesized that a very slow chemical degradation of ferricyanide due to cyanide loss may occur; however, they noted that their starting material contained pentacyanide impurities, thus calling into question whether any observed cyanide ligand loss was due to a spontaneous ferricyanide decomposition process, or decomposition promoted by the already present pentacyanides. They also noted that pentacyanides in solution can be rejuvenated back to ferrocyanide by the addition of free cyanide.

However, it is only recently that this coordination compound has been reported to appear extremely unstable in dark, alkaline, conditions at room temperature. A study by Luo et al. observed rapid capacity fade while cycling pH 14 ferri-/ferrocyanide electrolytes in a capacity-balanced compositionally symmetric cell, starting with one side fully charged and the other fully discharged (called “half-cells”).³³ The researchers attributed the decrease in capacity to chemical decomposition of ferri-/ferrocyanide via cyanide ligand dissociation from the iron center, and subsequent irreversible hydroxylation of the coordination compound. Soon after, Goulet and Aziz³⁴ reported the reduction of ferricyanide to ferrocyanide occurring when in contact with carbon paper electrodes, noting that the reaction rate appeared pH-dependent. More importantly, they did not observe irreversible chemical decomposition of ferri-/ferrocyanide in ex situ characterization of electrolytes cycled in volumetrically unbalanced compositionally symmetric cells, calling into question the results of Ref. 33. Cazot et al.³⁵ observed significantly lower capacity fade rates than those reported in Ref. 33, in ferri-/ferrocyanide capacity-balanced compositionally symmetric cells at high pH. They noted that fluctuating membrane resistance during cell cycling could partially explain the apparent fade demonstrated in Ref. 33 due to the use of purely galvanostatic cycling. Páez et al.³⁶ revisited the experiments performed in Ref. 33

*Electrochemical Society Student Member.

**Electrochemical Society Member.

^zE-mail: maziz@harvard.edu

and further disproved the claims of ferri-/ferrocyanide chemical instability in alkaline conditions. They also proposed that cell unbalancing due to the electrochemical oxygen evolution reaction (OER) could play an important role in the observed apparent cycling capacity fade, as previously hypothesized in Ref. 34.

Most recently, in a follow up to their previous work of Ref. 33, the Liu group once again reported findings³⁷ of cyanide ligand dissociation and subsequent irreversible hydroxylation but demonstrated this degradation mechanism only under conditions of addition of free cyanide in solution and of light illumination. However, they have revised their interpretation. The majority of observed capacity fade in capacity-balanced compositionally symmetric “half-cells” is now attributed to the chemical reduction of ferricyanide to ferrocyanide, balanced by graphite felt oxidation to carbonate (CO_3^{2-}) and ammonia. Once again, rapid apparent capacity fade was attributed in part to an irreversible chemical degradation, but *ex situ* ^{13}C NMR and UV–vis data were inconsistent with the apparent extreme loss of capacity. They further proposed that the previously observed parasitic reduction of ferricyanide to ferrocyanide in alkaline conditions is also partially balanced by a chemical oxidation of the proposed dissociated cyanide (CN^-) to cyanate (OCN^-). However, the validity of this mechanism hinges on the requirement for ample free cyanide to be present in solution and, if correct, the mechanism requires a more nuanced interpretation involving hydroxide to both fully balance the hypothesized chemical redox reaction and explain observed pH-dependence. Thus, the proposed mechanisms of Ref. 37 would be applicable to a flow battery utilizing ferri-/ferrocyanide electrolytes only if free cyanide is present in solution. Herein, we explain the results of Refs. 33 & 37 through a different mechanistic interpretation. Given that flow battery electrolytes are normally protected from light by their enclosing materials and that the instability of alkaline ferri-/ferrocyanide solutions in the presence of light has never been in question, it is the determination of structural stability in the dark that is most pertinent to a lifetime evaluation of the use of alkaline ferri-/ferrocyanide electrolytes in commercial flow batteries.

Unfortunately, many of these studies have not used potentiostatic holds on a volumetrically unbalanced compositionally symmetric cell setup, which we have argued^{8,13,34} to be the most robust configuration for evaluating molecular decomposition-based capacity fade rates and determining compositionally symmetric cell capacity fade mechanisms. A volumetrically balanced symmetric cell can exhibit apparent capacity fade, even if there is no structural degradation of redox-active species, if side reactions such as ferricyanide reduction to ferrocyanide occur, thereby shifting the accessible state-of-charge (SOC) range. Furthermore, purely galvanostatic cell cycling is subject to artifacts in accessed capacity due to drifts in internal polarization resistance.

We have re-examined the structural stability, in the dark, of ferri-/ferrocyanide in alkaline conditions using a series of experiments designed to unambiguously determine whether the measured capacity fade arises from irreversible chemical degradation or reversible chemical or electrochemical side reactions. Electrochemical and structural stability have been analyzed for both pristine electrolytes and electrolytes subjected to electrochemical cycling in flow cells. Coulometric analysis was first performed utilizing the volumetrically unbalanced compositionally symmetric cell technique.³⁴ The *ex situ* methods of NMR and UV–vis absorption spectrophotometry were employed to distinguish between structural degradation and apparent (electrochemically reversible) capacity fade. Our findings indicate that ferri-/ferrocyanide remains structurally stable in the dark in the tested range of pH 7–14, but that ferricyanide undergoes chemical reduction to ferrocyanide in alkaline conditions, accompanied by chemical oxidation of hydroxide to O_2 (chemical OER) acting as the balancing oxidation half-reaction. Notably, we find that the rate of the chemical redox reaction can increase markedly when an alkaline solution containing ferricyanide is in contact with porous carbon electrodes, without any applied potential. We also demonstrate that the electrochemical cycling of

alkaline ferri-/ferrocyanide electrolytes can be accomplished without promoting oxygen evolution from electrochemical splitting of water, suggesting that previous work³⁶ attributing capacity fade to the electrochemical OER, shifting the accessible SOC range and leading to cell unbalancing, requires a different interpretation. Our work suggests that cyanide ligand dissociation of ferri-/ferrocyanide is a photocatalytic process, rather than a mechanism occurring independent of light exposure as previously proposed in Refs. 33 & 37. We also describe how the rate of apparent capacity fade in ferri-/ferrocyanide volumetrically unbalanced compositionally symmetric cells depends on pH and the ratio of total ferricyanide to carbon electrode surface area, defined by the initial configuration of electrolyte reservoirs in a given cell. Based on these results, we have determined a set of conditions enabling the successful implementation of ferri-/ferrocyanide electrolytes in long duration energy storage applications. Furthermore, we demonstrate why a chemical reduction process in an electrolyte used extensively by the AORFB community typically avoids detection in standard full cell battery cycling. Our results provide insights into several approaches that may introduce artifacts that obscure the parasitic reduction process. Collectively, the results reported here should provide confidence to the AORFB community about the lifetime of ferri-/ferrocyanide as an alkaline posolyte species.

Experimental

Electrolyte preparation.—Reagents used to prepare electroactive (posolyte and negolyte) solutions were purchased from Sigma Aldrich and used with no further purification: potassium hydroxide, potassium ferrocyanide trihydrate (99.5% purity), and potassium ferricyanide (99.5% purity). Throughout the manuscript we will be referring to these chemicals as KOH, ferrocyanide, and ferricyanide, respectively. Because atmospheric CO_2 readily dissolves into high pH solutions, we prevented carbonate formation by storing and cycling our solutions in an oxygen/ CO_2 -free glovebox (O_2 partial pressure less than 2 ppm). Electrolyte solutions for cell cycling were also prepared inside the glovebox, using deoxygenated deionized water that had already equilibrated with the glovebox atmosphere over multiple months.

Electrode materials.—Two different commercial electrodes were used: Sigracet GDL 39AA (Fuel Cell Store), and AvCarb HCBA 1186 carbon cloth (AvCarb Materials Solutions). Hereafter we refer to these electrodes as SGL and HCBA, respectively. SGL has an uncompressed thickness of 280 μm and HCBA has an uncompressed thickness of 1.3 mm. All electrodes were baked at 400 °C in air for 24 h prior to use.

Cell assembly.—Flow battery experiments were carried out with cell hardware from Fuel Cell Technologies Inc. (Albuquerque, NM), assembled into a zero-gap flow cell configuration, as described in a previous report.² Pyrosealed POCO graphite flow plates (9 in²) with interdigitated flow patterns were used for both electrodes. Unless otherwise stated, each electrode comprised a 5 cm² geometric surface area covered by either a stack of two sheets of SGL, or one HCBA electrode, per side. The outer portion of the space between the electrodes was gasketed using Viton sheets (10 mils for SGL cells, 30 mils for HCBA cells) with the area over the electrodes cut out. The torque applied during cell assembly was 60 lb-in (6.78 N-m) on each of eight 3/8”–24 bolts, thus the load applied per bolt is approximately 800 lbs. Electrolytes were fed into the cell through fluorinated ethylene propylene (FEP) tubing at a rate of 60 ml min⁻¹, controlled by Cole-Parmer 6 Masterflex L/S peristaltic pumps. For all symmetric cell tests, a sheet of Nafion 117 (Ion Power Inc.) membrane served as the ion-selective membrane between the carbon electrodes. All membranes were presoaked in 1 M KOH for 3 d to ion exchange the counter ions from protons to potassium ions. If a membrane was to be tested in an electrolyte solution with a pH lower than 14, the membrane was then soaked for

an additional day in a KOH solution with the target pH, or deionized water for pH 7.

Cell cycling protocol.—Cycling stability of the ferri-/ferrocyanide electrolyte was studied by the volumetrically unbalanced compositionally symmetric cell method, as described elsewhere,³⁴ hereafter referred to as a symmetric cell. Unless otherwise stated, the capacity-limiting side (CLS) and non-capacity limiting side (NCLS) contained identical starting solution compositions, both initially at 50% SOC i.e., equal concentrations of ferricyanide and ferrocyanide. Charge/discharge cell cycling was performed using a Biologic VSP-300 potentiostat. All cells reported in this work were driven with a square wave in voltage with amplitude 200 mV, with 2 mA cm⁻² (geometric area) current cutoffs for reversing polarity. We always started the first cycle by reducing ferricyanide to ferrocyanide in the CLS. All cells were run inside a glovebox with minimal exposure to lab light.

¹³C NMR.—¹³C NMR spectra were taken from electrolyte solutions that were initially dissolved in D₂O as solvent, instead of H₂O, thus dilution for NMR was not required. All cycled CLS samples were electrochemically reduced to 100% ferrocyanide (Fe²⁺) in the reaction cell with a fresh NCLS, to avoid the signal interference from the paramagnetic ferricyanide (Fe³⁺). For each sample, a 650 μl aliquot was taken from the starting solution and 20 μl of DMSO-d₆ was added as internal standard to avoid chemical shift inconsistencies caused by sample preparation and different pH. All ¹³C NMR samples were scanned 2048 times at room temperature to collect final spectra in an Agilent 500 MHz NMR instrument.

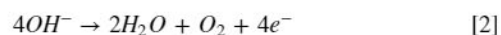
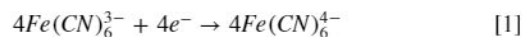
UV-vis spectrophotometry.—To confirm the structural stability of ferricyanide, a 0.5 mM solution of ferricyanide in 1 M KOH was prepared and fractionated into small vials of 3 ml. As reported in a previous publication,³⁴ the total iron concentration was measured with UV-vis spectrophotometry (Varian, Cary 60) at a wavelength of 278–282 nm (determined by instrument calibration) and the ferricyanide concentration at a wavelength of 420 nm. Since numerous studies have demonstrated that ferri-/ferrocyanide is susceptible to photocatalyzed decomposition^{30–32} all the experiments were performed protecting the solutions from light by wrapping the vials with aluminum foil and keeping them stored in a closed box in a lab with no windows. To study the effect of the carbon electrode interaction, the same starting solution was added to several vials (3 ml) containing sheets (4 mm × 4 mm) of SGL or HCBA electrodes.

Results

Effect of pH on ferri-/ferrocyanide cycling stability.—We first characterized the effect of pH on the observed capacity fade in symmetric cells by comparing four identical cell builds using SGL as electrodes, with 0.1 M ferri-/0.1 M ferrocyanide electrolytes at varying pH. As seen in Fig. 1, a clear drop in capacity is observed when cycling ferri-/ferrocyanide symmetric cell flow batteries at highly alkaline pH. We report instantaneous temporal fade rates derived from the slope of the natural log of reduction cycle capacity vs time plot (−d ln C/dt, where C(t) is the time-dependent reduction capacity). The plotted oxidation capacities in Fig. 1a represent 118, 123, 155, and 103 cycles for pH 7, 12, 13, and 14, respectively. We do not report AORFB capacity fade rates in units of % per cycle as it is a meaningless figure for time-denominated fade mechanisms when the cycle period changes due to a) ohmic resistance changes, and b) (apparent) capacity fade. Furthermore, comparing fade rates of cells that differ in initial capacity are meaningless if using % per cycle, unless the cycle period is identical between each cell. An increased rate of capacity fade with increase in pH can clearly be seen in Fig. 1, similar to the reported trend in Ref. 33. However, a distinct difference in total capacity utilization must first be noted between our work and previous work demonstrating cell cycling of AORFB

electrolytes. Each symmetric cell in Fig. 1 initially accesses >99% of the theoretical capacity of the CLS electrolyte due to the use of potentiostatic charge/discharge cycling. Both Refs. 33 & 37 cycle cells galvanostatically, consistently accessing less than 90% of their theoretical initial capacity, thus leading to inconsistent results associated with accessing the full SOC range. When comparing multiple different cells with presumably different cell ohmic resistances (typically membrane-dominated, especially across multiple pH values), galvanostatic cycling alone results in significantly different absolute values of accessed capacities, vitiating any cell capacity fade comparison made using such cycling techniques. Given that our volumetrically unbalanced compositionally symmetric cells begin initially at 50% SOC in the CLS and NCLS, and the CLS of each cell is reduced first, the first reduction capacity data point is roughly half of the total capacity (i.e., the CLS is reduced from 50% to 100% SOC) and the first oxidation capacity data point is ideally the total capacity (i.e., the CLS is oxidized from 100% to 0% SOC). Of note in Fig. 1, initial oxidation capacities of greater than 100% theoretical capacity are achieved, with increased capacity seen at increased pH—especially at pH 14 where 112% of theoretical capacity (115C) is achieved in the first oxidation half-cycle. If ferri-/ferrocyanide is structurally stable and these cells simply suffer from apparent capacity fade, this is an indication of the previously reported³⁴ pH-dependent parasitic reduction of ferricyanide to ferrocyanide. During oxidation, the CLS converts ferrocyanide to ferricyanide (facilitated electrochemically by the flow cell) but a chemical reduction of ferricyanide back to ferrocyanide could continually occur in solution if ferricyanide is present. We refer the reader to the schematic in Fig. S1 that traces the temporal evolution of accessed ferricyanide present in each reservoir during cycling, and how that relates to apparent capacity.

Given that the reduction potential of ferri-/ferrocyanide is pH-independent, high pH leads to increased favorability of the OER in a ferri-/ferrocyanide solution. This effect can be explained by examining the Pourbaix diagram for aqueous ferri-/ferrocyanide in Fig. 2, with half reactions of interest described by the following equations:



A subtle distinction to be considered is the Nernstian shift of the OER potential–pH equilibrium line as a function of oxygen partial pressure: assuming room temperature, the OER in air (21% oxygen) is shifted 10 mV more negative than standard conditions (i.e., 1 bar oxygen), and in glovebox (2 ppm oxygen) the OER is shifted 84 mV more negative than standard conditions. Thus, for a 50% SOC ferri-/ferrocyanide electrolyte, the oxidation of water accompanied by the reduction of ferricyanide to ferrocyanide is thermodynamically possible at pH >12.3 in air, or pH >11.1 in a glovebox with an O₂ partial pressure of 2 ppm. It should be noted, however, that electrochemically, the OER is kinetically so sluggish—especially on carbon electrodes—that it does not occur for several hundred mV higher than we ever expose this system to.³⁸

When cycling a symmetric cell starting at 50% SOC in both the CLS and NCLS (i.e., identical solutions except in volume), the initial open circuit voltage is 0 V, and a voltage of ±200 mV is applied across the cell for charge/discharge in order to access over 99% of the capacity of the CLS.³⁴ Given that both sides of the cell contain identical concentrations of the same starting electrolytes, it is reasonable to assume that the applied potential is equally divided between CLS and NCLS i.e., 100 mV of overpotential per side (see blue shaded region of Fig. 2 denoting ±100 mV window about the formal reduction potential of ferri-/ferrocyanide, resulting from an absolute applied voltage of 0.2 V on each charge/discharge cycle). A previous report attributes the observed capacity fade to electrochemical OER occurring concurrently with ferricyanide reduction during the discharging process.³⁶ However, the electrochemical OER is kinetically sluggish on carbon and would proceed only

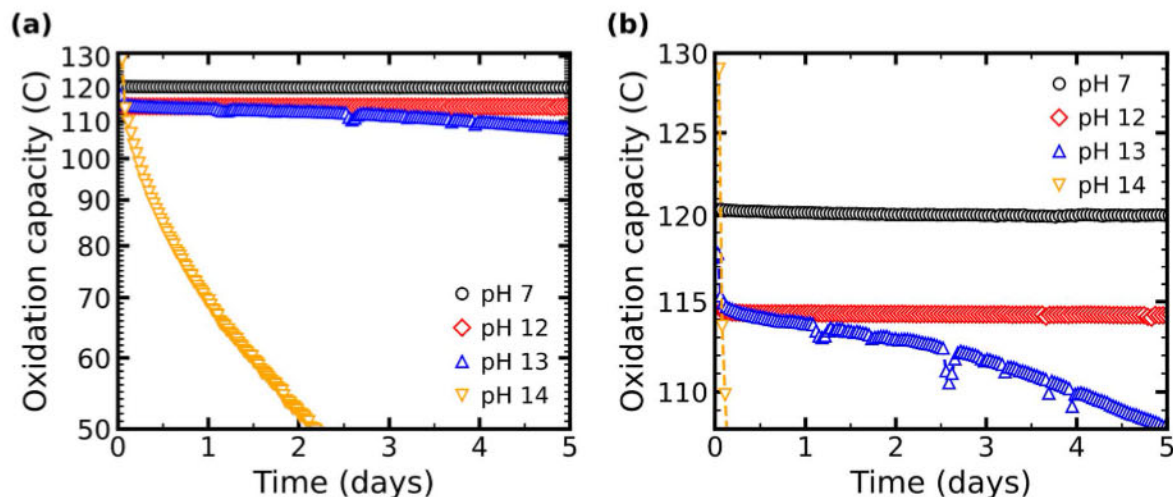


Figure 1. (a) Potentiostatic cycling of 0.1 M ferri-/0.1 M ferrocyanide at pH 7, 12, 13, and 14 in volumetrically unbalanced compositionally symmetric cells with SGL electrodes; pH 7 is 6.3 ml CLS vs 11.0 ml NCLS, while all other cells are 6.0 ml CLS vs 11.0 ml NCLS. (b) with zoomed in vertical scale.

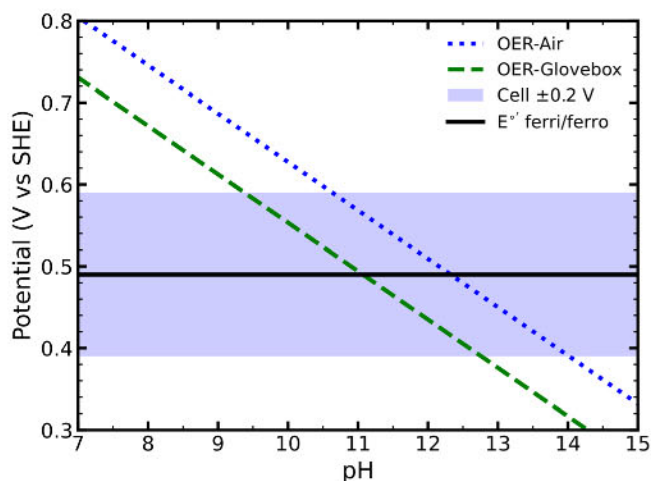


Figure 2. Pourbaix diagram of ferri-/ferrocyanide, oxygen evolution reaction (OER) in different atmospheres, and 200 mV window accessed by the symmetric cell when an initially 50% SOC solution is used as CLS and NCLS.

when a large overpotential is applied. This is inconsistent with the results of Goulet and Aziz,³⁴ in which fast capacity fade was still observed when pH 14 ferri-/ferrocyanide electrolytes were pumped through a cell without any electrochemical cycling, and capacity fade rates significantly decreased when electrolytes were stored out of contact with the electrodes of the cell for a period of time before cycling the cell again. The observed rapid reduction of ferricyanide in alkaline conditions is indicative of a chemical reduction, possibly catalyzed by carbon electrodes. Taken together, these results indicate that stable ferri-/ferrocyanide cycling without structural degradation is not limited to neutral pH.³⁹ Other examples of chemical OER facilitated by species with similar reduction potentials to ferri-/ferrocyanide include $\text{Au}(\text{OH})_4^-$,⁴⁰ and $\text{W}(\text{CN})_6^{3-}$ and $\text{Mo}(\text{CN})_6^{3-}$.⁴¹

Carbonate species vs free cyanide.—In the reported claim of alkaline ferri-/ferrocyanide chemical instability, Ref. 33, the supposed nail in the coffin was ^{13}C NMR detection of free cyanide. Rather than free cyanide, Páez et al. proposed that this signal arises from dissolved carbonate, which they hypothesized comes from K_2CO_3 impurity present in bulk dry KOH.³⁶ However, while we agree that carbonate is being detected instead of free cyanide, we

hypothesize that the main source of dissolved carbonate in both works is actually atmospheric in origin. ^{13}C NMR data from Ref. 36 demonstrate a carbonate signal that increased in intensity as the electrolyte was cycled in an RFB over time, analogous to the results in Ref. 33. Neither report makes any mention of the use of an inert glovebox atmosphere for both flow cell cycling and ^{13}C NMR sample preparation, leading us to hypothesize that atmospheric CO_2 could readily dissolve in the highly alkaline electrolytes as they cycled. CO_2 absorption into alkaline aqueous solutions is well-known, with the carbonate ion being the dominant carbon species at high pH, and bicarbonate ion dominating in mildly alkaline conditions. The analysis of cycled alkaline ferri-/ferrocyanide electrolytes is further complicated because in alkaline conditions, free cyanide has a ^{13}C NMR shift of 165–166 ppm,^{42,43} but between pH 7–14, the carbonate/bicarbonate peak ranges over 161–170 ppm, potentially overlapping the cyanide signal.⁴⁴ The range in signal shift is due to the fast equilibration of carbonate/bicarbonate which results in a single NMR peak whose chemical shift depends on the relative concentration of the two species, which is a function of pH.⁴⁵ This explains the carbonate/bicarbonate peak and lack of free cyanide peak observed in ^{13}C NMR data from Ref. 36, and the peak misattributed to free cyanide in Ref. 33. Results from cycled ferri-/ferrocyanide electrolytes at pH >14 also show the same issue of carbonate being mistaken for cyanide.⁴⁶

To confirm the structural stability of alkaline ferri-/ferrocyanide electrolytes under our cycling conditions, we measured the ^{13}C NMR of the pH 14 electrolyte solutions for CLS and NCLS reservoirs before and after the cycling that showed dramatic capacity fade in Fig. 1. No dissolved carbonates were detected in cycled electrolytes from cells with SGL or HCBA electrodes. However, when performing these cycling experiments again with electrolytes using D_2O as initial solvent (i.e., no dilution of aliquots required for NMR measurements), a small amount of dissolved carbonate was detected in cycled electrolyte from a cell with SGL electrodes. In Fig. 3 we show ^{13}C NMR spectra, with controls for free cyanide with a signal at 164.9 ppm, dissolved carbonate (168.9 ppm), and uncycled ferrocyanide (176.8 ppm), all at pH 14 in D_2O . Ferricyanide is a paramagnetic species and is not detected in standard ^{13}C NMR; the presence of small amounts of ferricyanide inhibits the carbon signal from ferrocyanide, as shown in Ref. 36. The unpaired electron in ferricyanide causes considerable line broadening of NMR signals from nuclei close to Fe^{3+} due to its shorter electron relaxation time. Consequently, the ^{13}C NMR signal of ferricyanide is too broad to be seen. Therefore, measuring ^{13}C NMR of cycled ferri-/ferrocyanide electrolytes without first ensuring a fully reduced (i.e., all

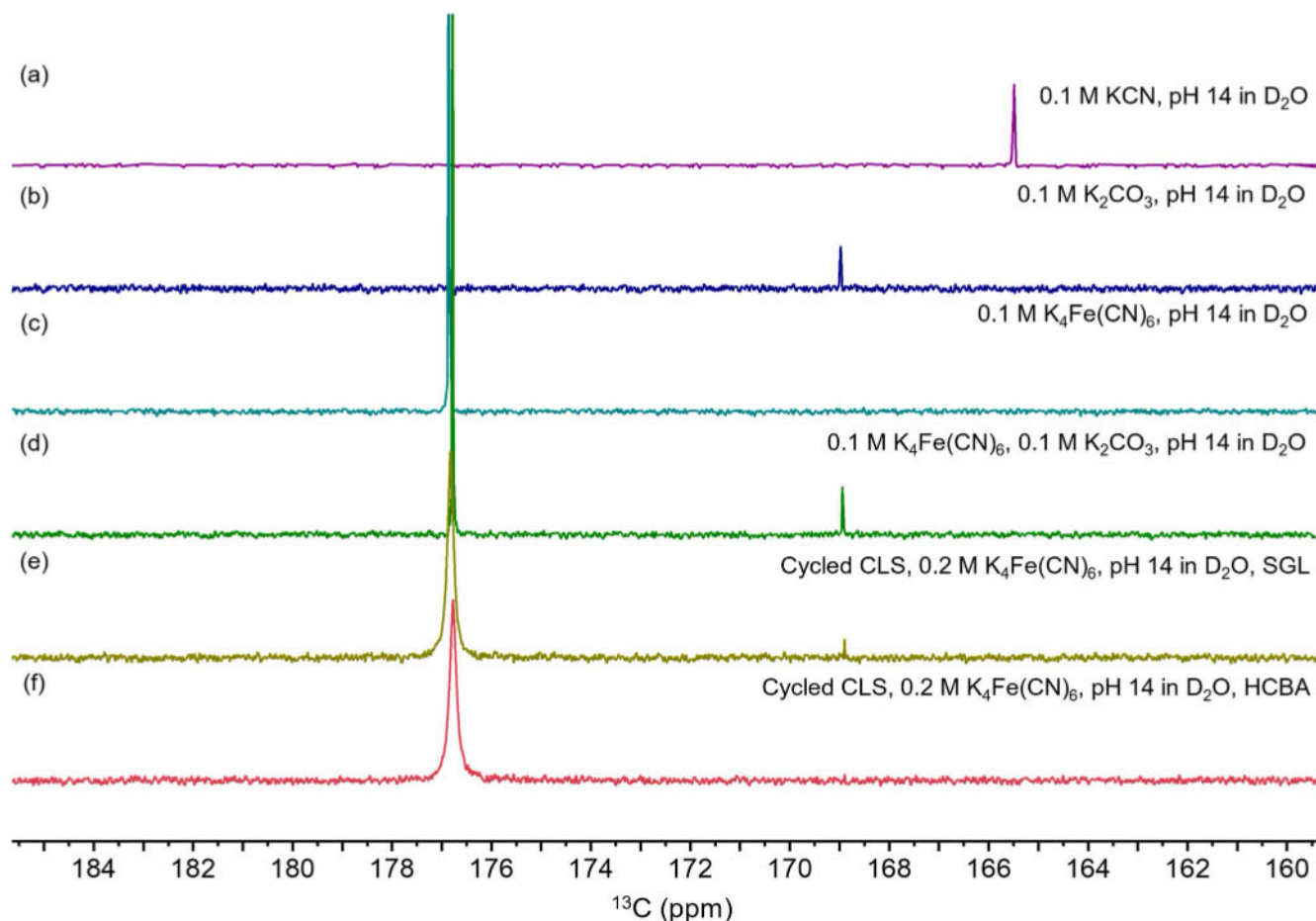


Figure 3. ^{13}C NMR measurements of (a) 0.1 M potassium cyanide at pH 14; (b) 0.1 M potassium carbonate at pH 14; (c) uncycled 0.1 M ferrocyanide at pH 14; (d) 0.1 M ferrocyanide, 0.1 M potassium carbonate at pH 14; (e) Electrolyte from CLS of 0.1 M ferri-/0.1 M ferrocyanide pH 14 symmetric cell with SGL electrodes, electrochemically cycled for 7 d, and then fully reduced to ferrocyanide; (f) Electrolyte from CLS of 0.1 M ferri-/0.1 M ferrocyanide pH 14 symmetric cell with HCBA electrodes, electrochemically cycled for 7 d, and then fully reduced to ferrocyanide. All electrolytes used D_2O as initial solvent i.e., no dilution was required for NMR. The signal at 176.8 ppm corresponds to diamagnetic ferrocyanide. An extended view of the spectra is shown in Fig. S2.

ferrocyanide) sample would likely not deliver any carbon signal from ferri-/ferrocyanide. Combined with the presence of undesired dissolved CO_2 species (as described earlier) one could be led to incorrectly conclude that ferri-/ferrocyanide has fully degraded and released its cyanide ligands into solution, as we hypothesize occurred in Ref. 33. Cycled electrolyte from the CLS of a symmetric cell with SGL electrodes demonstrates a small carbonate peak in Fig. 3e, but no carbonate is seen in cycled electrolyte from the CLS of a symmetric cell with HCBA electrodes, shown in Fig. 3f. However, we must note that by cycling electrolytes in D_2O rather than H_2O , we may introduce a kinetic isotope effect that could alter the rate of parasitic oxidation reactions. Though not a direct indication of reaction rate, cells with SGL electrodes cycling 0.1 M ferri-/0.1 M ferrocyanide pH 14 electrolytes with H_2O as solvent demonstrated an apparent capacity fade rate of $\sim 20\%/d$, while those with D_2O as solvent demonstrated an apparent capacity fade rate of $\sim 28\%/d$. Identical cycling experiments with HCBA electrodes resulted in apparent capacity fades of 0.1%/d and 0.5%/d for electrolytes with H_2O and D_2O solvents, respectively. The distinct difference in chemical shift between ferrocyanide, carbonate, and free cyanide indicates that the ferri-/ferrocyanide alkaline electrolyte did not chemically decompose to produce cyanide anions when cycled electrochemically in a symmetric cell with either SGL (Fig. 3e) or HCBA (Fig. 3f) electrodes. This is consistent with recent reports^{34,36} and confirms that the apparent capacity fade observed during cell tests is not linked to chemical decomposition of ferri-/ferrocyanide.

In recent work, a mechanism involving chemical ferricyanide reduction facilitated by cyanide oxidation to cyanate (OCN^-) was proposed.³⁷ The evidence for this process appears to be derived from misinterpreted ^{13}C NMR spectra, where the detection of cyanate (normally found near 129 ppm^{47,48}) is simply a result of the artificial addition of free cyanide into the alkaline electrolytes, followed by oxidation to cyanate. Given that the chemical reduction of ferricyanide is already being facilitated by the chemical OER, the presence or absence of cyanide in solution would not affect the final result of conversion to ferrocyanide. Furthermore, Ref. 37 claims that ammonia/ammonium was detected in ferri-/ferrocyanide electrolytes, thus proving their hypothesized mechanism of chemical ferricyanide reduction via cyanide oxidation to cyanate, which further hydrolyzes to ammonium. We offer an alternative explanation for these results. Their method of adding 2 M HCl to a solution of ferri-/ferrocyanide to trap ammonia (which evolves under the proposed mechanism) leads to a self-fulfilling prophecy: strong acid could in fact both release cyanide ligands from ferri-/ferrocyanide and hydrolyze the resulting free cyanide to ammonium formate. Acid-mediated hydrolysis of cyanide to ammonium formate is well documented,^{49–51} thus the proposed chemical reduction of cyanide to cyanate, further hydrolyzed to ammonia, may be incorrect in Ref. 37. This would explain the eventual detection of ammonia/ammonium and formate through the combination of ex situ ^1H NMR/ ^{13}C NMR/GC-FID results in Ref. 37. Hydrolysis of cyanide to ammonium can also be expedited by heating,⁵² and Ref. 37 detected ammonia by using GC-FID which heats the solution to several

hundred degrees Celsius. Furthermore, Ref. 37 did not state that the pH of all solutions tested by GC-FID are the same, thus any trend of ammonia concentration cannot necessarily be determined, as ammonia volatility is extremely pH-dependent. We performed ^1H NMR measurements of cycled ferri-/ferrocyanide pH 14 electrolytes and no ammonia was measured with a detection limit of 0.05 mM, as seen in Fig. S3. Note that unlike in Ref. 37, we did not add strong acid prior to NMR measurements as it will facilitate the release of free cyanide from ferri-/ferrocyanide.

In Fig. 3c, the absence of a signal from uncycled ferrocyanide electrolyte between 161–170 ppm indicates that we have prevented absorption of atmospheric CO_2 , which would result in dissolved carbonates and obfuscate any detection of free cyanide. Given that we do not observe free cyanide or dissolved carbonates in fresh electrolytes, or ammonia in cycled electrolytes exhibiting large apparent capacity fade, our results clearly undermine the proposed mechanisms in Refs. 33 and 37, and are a strong indication that alkaline ferri-/ferrocyanide electrolytes are structurally stable for RFB applications.

Carbon electrode-catalyzed chemical redox.—To quantitatively measure the stability of ferricyanide and its previously hypothesized interaction with porous carbon electrodes,³⁴ we used UV–vis spectrophotometry to measure total ferricyanide and total iron concentrations over time in quiescent solutions with and without SGL carbon electrodes. In Fig. 4 we report the resulting changes in ferricyanide and total iron concentration for a series of pH 14 solutions (initially 0.5 mM ferricyanide, hence 0.5 mM iron) stored either in contact or out of contact with SGL electrodes. Total iron concentration (measured by UV–vis) remains constant during both experiments, while the ferricyanide concentration decreases to almost zero in less than a week when the solution is in contact with the electrode. This demonstrates that there is a direct interaction between the carbon surface and ferricyanide. At high pH, the carbon electrode appears to enhance the rate of chemical ferricyanide reduction to ferrocyanide facilitated by the chemical OER, as previously reported.³⁴ However, a relatively slow chemical reduction of ferricyanide was still observed in solutions that were not in contact with the carbon electrodes, at a rate of 3%/d for a 3 ml sample of 0.5 mM ferricyanide at pH 14. Further investigation of the

chemical redox process at more commercially relevant electrolyte concentrations is shown in Fig. S4. Over a span of 45 d, instantaneous chemical reduction rates of $0.023 \pm 0.006\%/d$ and $0.017 \pm 0.004\%/d$ were measured for pH 14 solutions of 0.1 M and 0.2 M ferricyanide, respectively. We also show in Fig. S5 that the pH 14 solutions of 0.1 M and 0.2 M ferricyanide left in lab light will begin to form rust-colored precipitates (also reported by others³⁷) but when kept in the dark for multiple months, no precipitates are observed. In the dark and in absence of electrode contact, the rate of chemical ferricyanide reduction will ultimately set a pH-dependent upper limit on the lifetime for any RFB configuration, because this is the rate of ferricyanide reduction for electrolytes pumped out of the stack and stored in RFB tanks. Understanding how this rate depends on pH, concentration of ferri-/ferrocyanide, oxygen partial pressure in the headspace, and mixing properties of the electrolyte is an important direction for future work. Impurities in ferricyanide/KOH may also affect the rate of chemical OER, as has been shown in the case of chemical hydrogen evolution in certain RFB negolytes.^{36,53,54}

In the supplementary information (see Fig. S6) we report the results of the same experiment but with more oxygen-permeable polypropylene vials and observe that those solutions exhibit faster reduction of ferricyanide due to evolved oxygen escaping the vials more quickly. This suggests that the chemical OER (Eq. 2) raises the oxygen partial pressure in the head space, which acts to suppress the chemical OER rate unless O_2 escapes from the head space. To test this hypothesis, we employed gas chromatography-mass spectrometry (GC-MS) to detect the formation of O_2 . Three samples were prepared in glovebox: (a) 5 ml of 1 M KOH; (b) 5 ml of 0.25 M ferricyanide in 1 M KOH; (c) 5 ml of 0.25 M ferricyanide in 1 M KOH soaking a 5 cm^2 SGL carbon electrode. All solutions were sealed in 10 ml air-tight headspace vials for GC-MS measurements. Figures S7 & S8 show that an oxygen signal was detected from sample (b) and (c), which is consistent with Eqs. 1 and 2 stating that hydroxide is oxidized to O_2 while ferricyanide is reduced to ferrocyanide. Furthermore, a stronger oxygen signal (higher signal/noise ratio) is detected from sample (c), implying that the carbon electrode plays a role in catalyzing this chemical redox reaction. Additionally, the ^{13}C NMR spectrum of post-cycled ferri-/ferrocyanide electrolyte (traces e and f in Fig. 3) shows a small amount of

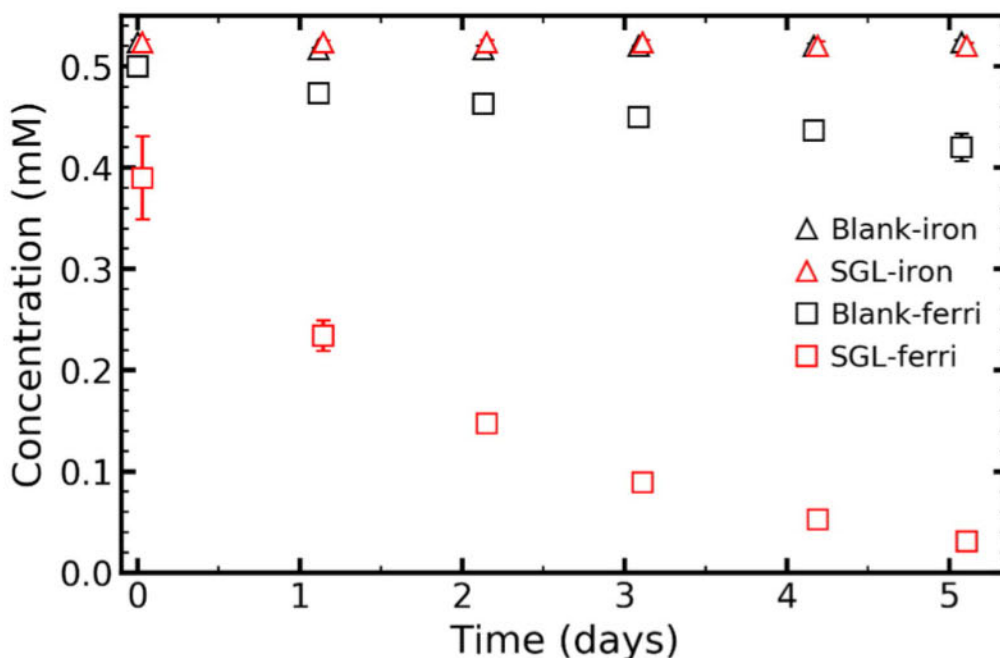


Figure 4. UV–vis measured time-dependence of ferricyanide and total iron concentration in 3 ml of 0.5 mM ferricyanide pH 14 solution in contact and out of contact with 4 mm × 4 mm SGL electrode. Solutions were stored in glass vials.

carbonate from electrolyte cycled in a cell with SGL electrodes, but no detected carbonate in electrolyte cycled in a cell with HCBA electrodes. The lack of any detected ammonia in cycled alkaline electrolytes experiencing significant apparent capacity fade contradicts the claims of chemical ferricyanide reduction being balanced by graphite felt oxidation and ammonia in Ref. 37. Therefore, both in situ (cell cycling) and ex situ (^{13}C NMR, UV-vis, GC-MS) experiments support the hypothesis of a pH-dependent chemical reduction of ferricyanide accompanied by chemical OER, which can be further accelerated by carbon electrodes. The recent report³⁷ proposing chemical reduction of ferricyanide facilitated in part by free cyanide oxidation detected minimal amounts of evolved O_2 in ferri-/ferrocyanide electrolytes but one possible reason for this is that their GC experiments were performed only on post-cycled electrolytes, when chemical OER may already have ceased after reaching equilibrium. It is also understandable that with a continuously flowing electrolyte, unsealed reservoir headspace, and gas permeable flow cell equipment, small amounts of oxygen evolution could go unnoticed and escape from lab-scale flow cells. Ref. 37 also proposes an additional mechanism involving chemical reduction of ferricyanide, balanced by graphite felt oxidation to carbonate and ammonia. Again, this is contradicted by our lack of detection of ammonia.

Electrode surface area.—The results of the previous section suggest a potential issue for RFB design when employing ferri-/ferrocyanide electrolytes and carbon electrodes. To explore the effect of electrode surface area, we utilized a porous electrode with the same geometric surface area as SGL but nearly five times lower specific surface area, the HCBA woven carbon cloth. Symmetric cell cycling of 0.1 M ferri-/0.1 M ferrocyanide solutions at different pH with HCBA electrodes is shown in Fig. 5, with the pH 14 SGL cycling data from Fig. 1 included as a comparison. The plotted oxidation capacities of HCBA cells in Fig. 5a represent 250, 255, and 201 cycles for pH 12, 13, and 14, respectively. Once again, each symmetric cell in Fig. 5 initially accesses >99% of the theoretical capacity of the CLS electrolyte due to the use of potentiostatic oxidation/reduction cycling. As seen in Fig. 1, cells using SGL electrodes often demonstrated initial oxidation capacities greater than 100% theoretical capacity, with increased initial capacity seen at increased pH, which is consistent with a chemical reduction of ferricyanide to ferrocyanide during electrochemical CLS oxidation. In the HCBA cells of Fig. 5, this effect is no longer seen in the oxidation capacity data. During symmetric cell cycling using SGL electrodes, a fast apparent capacity fade rate of roughly 20%/d was observed at pH 14, but when cells were cycled using

HCBA electrodes and pH 14 conditions only a minimal 0.1%/d apparent capacity fade rate was measured. Table 1 illustrates the increase in instantaneous apparent capacity fade rate with increasing pH for the symmetric cells of Figs. 1 & 5. Instantaneous apparent capacity fade rates are derived from the slope of the natural log of reduction cycle capacity vs time plot, averaged over the entirety of each experiment. These results imply that the coupled chemical ferricyanide reduction/OER reaction is enhanced by carbon electrode surface area, and therefore influences apparent capacity fade rates in symmetric cells.

We also measured the pH, before and after cycling, of the CLS electrolytes in SGL and HCBA cells, reported in Fig. 6 as total decrease in hydroxide concentration. 0.1 M ferri-/0.1 M ferrocyanide solutions at the given pH values were used as controls to monitor the coupled chemical ferricyanide reduction/OER without enhancement from contact with carbon electrodes, all kept and measured in glovebox. At each starting pH, the symmetric cells using SGL electrodes demonstrated larger loss of hydroxide than HCBA cells, but the use of either electrode led to a larger decrease in hydroxide concentration than the respective blank. For cycled electrolytes at pH 12, 13, and 14, the SGL cells experienced a decrease in initial hydroxide concentrations of approximately 0.008 M (80%), 0.057 M (57%), and 0.199 M (20%), respectively. All values in Fig. 6 are tabulated in Table SI.

^{13}C NMR measurement was performed for cycled 0.1 M ferri-/0.1 M ferrocyanide pH 14 electrolyte with D_2O as initial solvent, when HCBA was used as the electrode (analogous to the SGL measurement seen in Fig. 3e). ^{13}C NMR spectra of (reduced) CLS electrolyte from the HCBA cell is shown in Fig. 3f. Consistent with the results from SGL electrodes, we do not detect any formation of free cyanide in electrolytes cycled with HCBA electrodes, providing further evidence that the capacity fade observed during cell tests is only apparent and is not linked to structural decomposition of ferri-/ferrocyanide. Dissolved carbonates were not detected in the cycled CLS from the cell with HCBA electrodes, ruling out any process involving ferricyanide reduction facilitated by carbon electrode corrosion and ammonia formation in alkaline conditions as claimed in Ref. 37. UV-vis measurements of total ferricyanide and total iron concentrations over time in pH 14 electrolyte-soaked HCBA electrodes (analogous to the experiments performed in Fig. 4 for SGL electrodes) can be seen in Fig. S9. A trend of increased ferricyanide chemical reduction rate in the presence of carbon electrodes was again observed. However, it should be noted that the rate of ferricyanide chemical reduction in these ex situ measurements cannot easily be compared to the observed apparent capacity fade rates in cell cycling because the UV-vis measurements are in

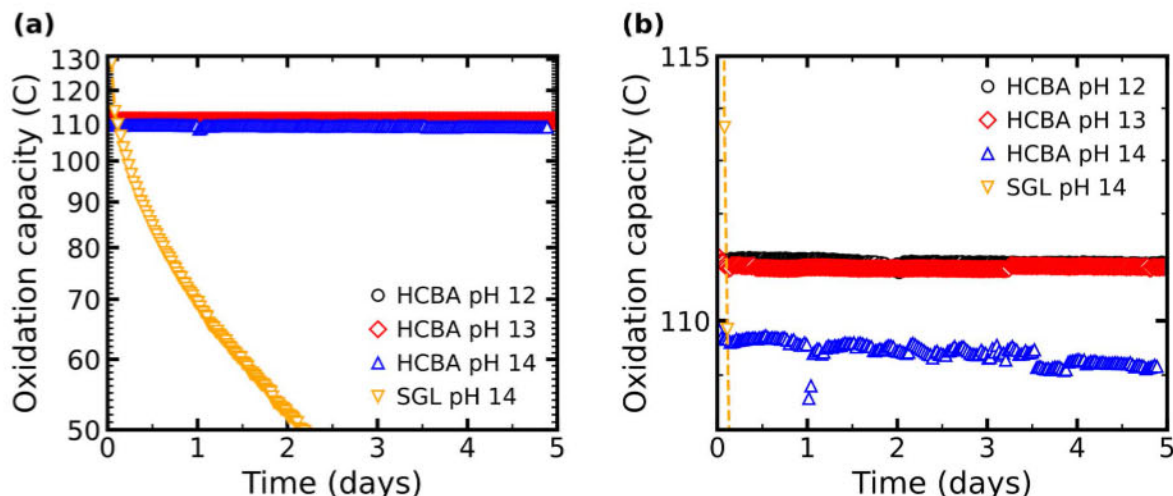
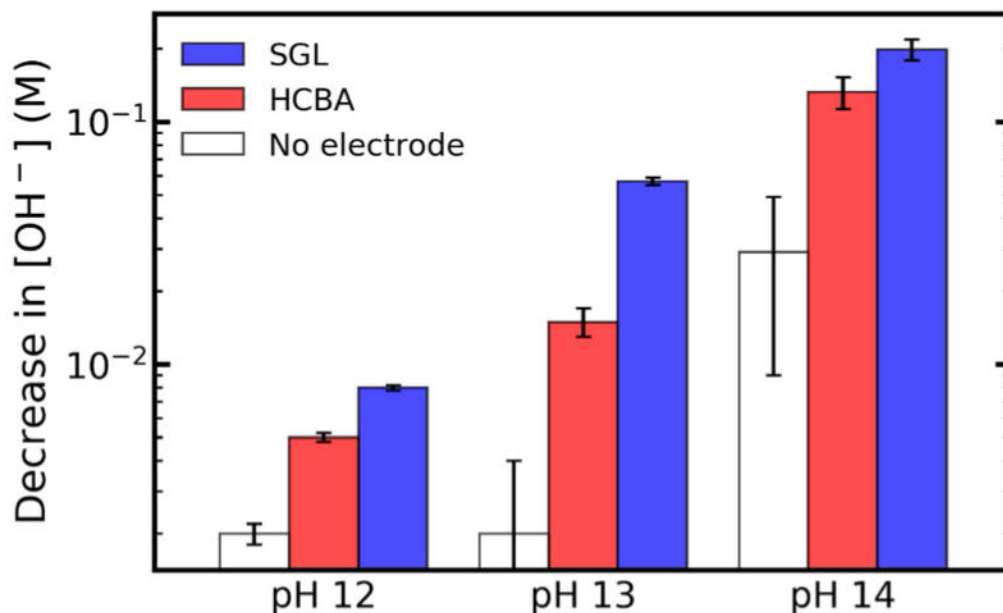


Figure 5. (a) Potentiostatic cycling of 0.1 M ferri-/0.1 M ferrocyanide at pH 12, 13, and 14 in volumetrically unbalanced compositionally symmetric cells with HCBA electrodes; pH 12 and 13 are 5.8 ml CLS vs 11.0 ml NCLS, pH 14 is 5.7 ml CLS vs 11.0 ml NCLS. Cell data for pH 14 with SGL electrodes from Fig. 1 is included as comparison. (b) with zoomed in vertical scale.

Table 1. Instantaneous apparent capacity fade rates of 0.1 M ferri-/0.1 M ferrocyanide symmetric cells, nominally 6 ml CLS vs 11 ml NCLS, cycled in glovebox.

pH	Instantaneous apparent capacity fade rate (%/day)	
	SGL	HCBA
7	none	—
12	<0.01	<0.01
13	1.4	0.01
14	20	0.1

**Figure 6.** Decrease in hydroxide concentration in the CLS of the volumetrically unbalanced compositionally symmetric cells from Figs. 1 & 5, measured after 5 d of cycling in a glovebox. “No electrode” is a 0.1 M ferri/0.1 M ferrocyanide solution at the given pH, identical to the starting CLS of each cell, left stirring in glovebox but without any contact with a carbon electrode.

quiescent solutions, compared to constant electrolyte flow in cells, and the act of electrochemically charging/discharging electrolytes in symmetric cells enforces a non-linear temporal electrochemical replenishment of a reactant i.e., ferricyanide. Furthermore, we cannot compare the rates of ferricyanide reduction between the two electrodes in the ex situ UV-vis experiments, because the use of quiescent solutions results in diffusion-limited reactions controlled by the intricate porous structures of the electrodes, which differ considerably.

To compare the available active sites of SGL and HCBA electrodes that enhance the coupled chemical reduction of ferricyanide and chemical OER is beyond the scope of this work as it would involve the combined characterization of hydraulic permeability and mass transport within the electrodes, the effect (if any) of electrode surface functional groups and/or doping on liquid/gas interactions, O₂ diffusion in the electrode, electrode compression, and electrochemically active surface area for the desired ferri-/ferrocyanide redox reaction.^{55–60} As a simplification, in Table SI we report BET surface area from gas adsorption measurements as an estimate of maximum available surface area for enhancement of the chemical redox process. We observe SGL to have nearly an order of magnitude larger specific surface area than HCBA.

Another issue with the SGL carbon electrodes is the graphitic binder that holds the intricate system of carbon fibers in place. This is contrasted by the HCBA electrodes fabricated by inter-weaving carbon fibers to provide mechanical strength without the need for a binder. SEM images of both electrodes are shown in Fig. S10, along

with EDS analysis with the elemental composition for SGL (Fig. S11) and HCBA (Fig. S12). Because of the manufacturing process, the HCBA electrodes are thicker than the SGL electrodes but have lower surface areas. We find that when cycling pH 14 ferri-/ferrocyanide electrolytes in symmetric cells using SGL electrodes, loss of carbon fibers can occur during cycling and can be seen by the change in color of the electrolyte solutions, which become darker. When left in quiescence for a few days after cycling, black fibrous deposits became apparent on the bottom of the electrolyte reservoirs, as shown in Fig. S13, indicative of fiber/binder removal from the electrode. The use of high surface area porous electrodes with binders complicates matters as the OER process can be mechanically destructive (gas generation in liquid-filled pores), causing the binder

to disintegrate over time and releasing electrode fibers. SGL is a gas diffusion electrode (GDE) optimized for gas flow in polymer electrolyte fuel cells, rather than liquid flow in an RFB, thus mechanical removal of degraded binder facilitated by constant electrolyte flow through the electrodes could occur. In the case of SGL electrodes, the ¹³C NMR-detected dissolved carbonates, likely due to chemical carbon oxidation, may originate from the graphitic binder itself which will further promote mechanical disintegration of the electrode. Much of the work in AORFBs has been built using the adopted architecture of fuel cells, especially the use of GDEs to provide high active surface area to facilitate the electrochemistry of dissolved redox-actives.⁶¹ Only recently has it been shown that carbon cloth electrodes may provide improved performance for RFBs in terms of electrochemical and hydraulic performance.^{56,57,62} A potential future tradeoff in electrode design can be envisaged between other design parameters to provide adequate electrokinetic, mass transport, and hydraulic performance, and decreasing surface area to cut the rate of electrode-enhanced ferricyanide chemical reduction.

Choose your own apparent capacity fade rate.—To distinguish coulometrically between irreversible chemical decomposition and apparent capacity fade due to electrode-enhanced chemical ferricyanide reduction, a 0.1 M ferri-/0.1 M ferrocyanide pH 14 symmetric cell with SGL electrodes was cycled for approximately four days, resulting in significant apparent capacity fade, as seen in Fig. 7. Electrochemical cycling was then paused, and the NCLS was

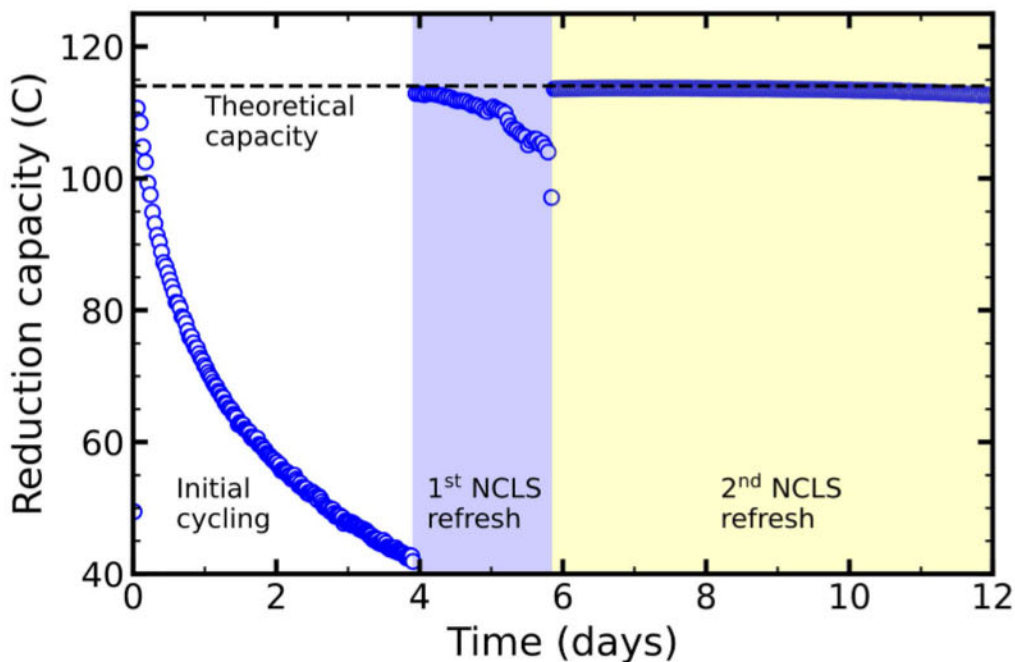


Figure 7. Potentiostatic cycling of a 0.1 M ferri-/0.1 M ferrocyanide pH 14 volumetrically unbalanced compositionally symmetric cell (6 ml CLS vs 11 ml NCLS) with SGL electrodes. The NCLS was replaced after approximately 4 d, and 6 d, with 11 ml of fresh 50% SOC electrolyte. The CLS is fully reduced prior to NCLS replacement.

replaced with a fresh electrolyte identical to the starting NCLS i.e., 50% SOC, 0.1 M ferri-/0.1 M ferrocyanide at pH 14. Electrochemical cycling was then restarted and maintained for two days before a second NCLS refresh occurred. Prior to the NCLS refreshes, the first CLS reduction delivered only 49C, which is less than half the total expected capacity of 115C ($\sim 57C$ expected from a 50% SOC CLS). Additionally, the first oxidation was greater than theoretical (120C measured). When considering the initial CLS oxidation of $>100\%$ theoretical capacity (explained previously, seen in Fig. 1), each successive NCLS refresh allowed for full capacity recovery in the CLS. Each successive run demonstrated a significant decrease in the instantaneous apparent capacity fade rate: $\sim 20\%/d$ during initial cycling, $\sim 5\%/d$ after the first NCLS refresh, and $\sim 0.1\%/d$ after the second NCLS refresh. We attribute this change in apparent capacity fade rate primarily to the continuous decrease in CLS pH due to chemical OER/carbon oxidation, the rate of which decreases over time as pH drops. Although we refresh the NCLS with a new pH 14 solution, the NCLS does not spend as much time as does the CLS at extreme SOC values where ferricyanide is high in concentration (see schematic of Fig. S1). The loss of SGL fibers, due to chemical/mechanical degradation of the binder, should not significantly affect total available surface area for parasitic chemical oxidation but it will decrease total available surface area for cell-based faradaic electrochemistry. This may also contribute to the decreased apparent capacity fade rate over time. The data in Fig. 7 prior to the first NCLS refresh are similar to those previously published^{33,37} for alkaline ferri-/ferrocyanide cells where the authors concluded in each case that extreme capacity fade was due to irreversible chemical degradation, rather than checking whether cell unbalancing had occurred and all initial capacity actually remained. We also carried out a similar experiment with a 0.05 M ferri-/0.05 M ferrocyanide pH 14 electrolyte, which demonstrated an apparent capacity fade rate of $120\%/d$ during initial cycling. Once again, we were able to fully achieve the initial CLS capacity after significant apparent capacity fade by refreshing the NCLS. We refer the reader to Fig. S14 for details.

Given that the parasitic side reaction is the reduction of ferricyanide to ferrocyanide, the time-dependence of the reduction capacity of a fully oxidized electrolyte reflects only the loss rate of the active species,

whereas the time-dependence of the oxidation capacity reflects additionally the relative rates of parasitic reduction reaction and electrochemical oxidation. That is, one may obtain arbitrary values of the oxidation capacity by manipulating electrical current and factors that influence the rate of the parasitic side reaction. Consequently, we plot reduction capacity in Fig. 7 to assess the decomposition rate of ferri-/ferrocyanide, and elsewhere we plot oxidation capacity to illustrate the influence of the parasitic reduction reaction.

Measured capacity fade can be apparent but not due to actual structural degradation, and Fig. 7 highlights the impact of a diminishing accessible SOC range in both the CLS and the NCLS. Whenever a parasitic reduction reaction is possible, the NCLS should have excess oxidized species beyond those barely required to oxidize all reduced species in the CLS, and whenever a parasitic oxidation reaction is possible, the NCLS should have excess reduced species. Other proposed “half-cell” configurations do not provide this safety buffer, and their use has resulted in the misinterpretation of apparent capacity fade rates as structural degradation.^{33,37,63}

The effect of the chemical ferricyanide reduction at pH 14 with SGL electrodes was then evaluated in terms of flow battery relevant design metrics, such as number of electrode sheets per geometric surface area and electrolyte volumes in the CLS and NCLS. Figure 8 demonstrates the effect of increased electrode surface area on the apparent capacity fade rate, in cells containing a fixed electrolyte concentration (0.1 M ferri-/0.1 M ferrocyanide, at pH 14), with varying number of sheets of SGL electrodes on both sides of the cell. As the ratio of carbon electrode active surface area to concentration (or moles) of ferri-/ferrocyanide increases, the apparent capacity fade rate increases. Commercial scale AORFBs built for long duration energy storage would likely employ very large electrolyte volumes and active species concentrations for high energy density, and thus would have very small ratios of electrode active area to moles of ferri-/ferrocyanide, thereby decreasing apparent capacity fade rates (if any) attributed to the posolyte chemistry. The absence of such apparent fade rates can already be seen in numerous reports of extremely low capacity fade rates of negolyte chemistries cycled against alkaline ferri-/ferrocyanide posolytes with very small electrode area to moles ferri-/ferrocyanide ratios.^{8,10,13,14,64,65}

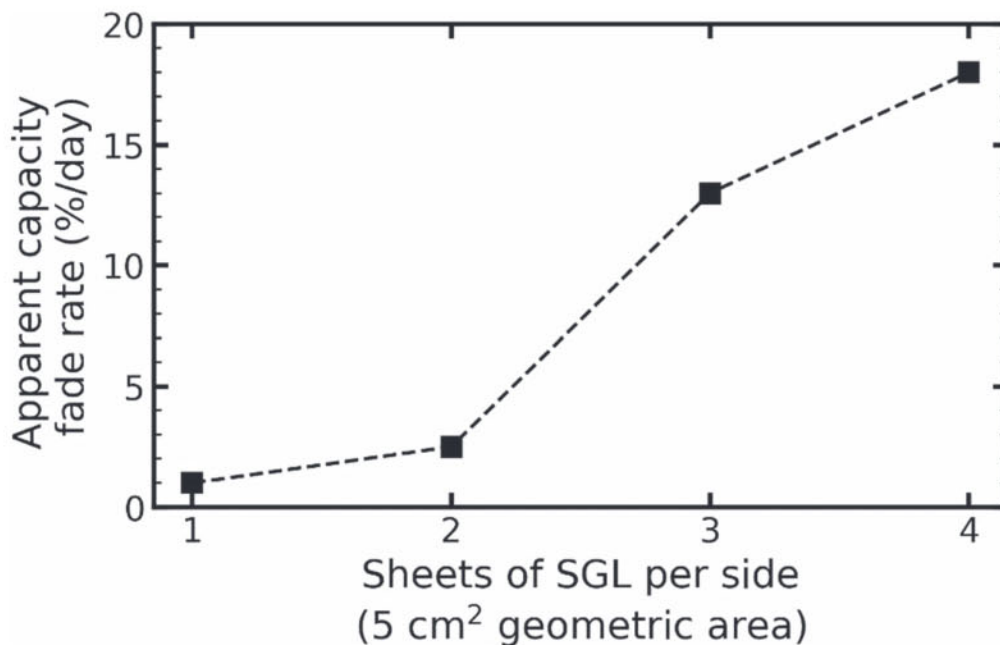


Figure 8. Apparent capacity fade rates of potentiostatically cycled 0.1 M ferri-/0.1 M ferrocyanide pH 14 volumetrically unbalanced compositionally symmetric cells (12 ml CLS vs 22 ml NCLS) with a varying number of sheets of SGL electrodes per side. Lines are meant only to guide the eye.

The volume of electrolytes in the CLS and NCLS, through their ratio, define the allowable trajectory of accessible SOC when cycling ferri-/ferrocyanide symmetric cells experiencing chemical reduction of ferricyanide. For example, a larger NCLS:CLS volume ratio results in a smaller change in the NCLS SOC during cycling. To demonstrate the effect of reservoir volumes, we cycled 0.1 M ferri-/0.1 M ferrocyanide pH 14 electrolytes in cells with SGL electrodes at multiple NCLS volumes with a fixed 4 ml CLS, as seen in Fig. 9. We first note that apparent capacity fade rates increase as NCLS volumes decrease. Given the fixed CLS volume in each cell, this means that a smaller difference between volumes of the CLS and NCLS leads to faster apparent capacity fade rates. This trend occurs due to the smaller NCLS volumes having to swing to larger SOC

extremes to enable access to CLS capacity. The deeper the SOC swings in the NCLS, the larger is the peak concentration of electrochemically generated ferricyanide. A higher concentration of ferricyanide could lead to a faster rate of chemical reduction of ferricyanide, furthering cell unbalancing due to the NCLS becoming capacity-limiting more rapidly, but we note that the apparent capacity fade rate itself is a complicated function of the initial setup of the symmetric cell. The theoretical capacity of all cells in Fig. 9 is 77C, yet a capacity greater than 100% of the theoretical value is achieved in the first oxidation cycle of all cells except that with the smallest NCLS volume (6 ml). We refer the reader to Fig. S1 for an explanation of how this excess measured oxidation capacity is achieved. As the NCLS volume is increased in the cells of Fig. 9,

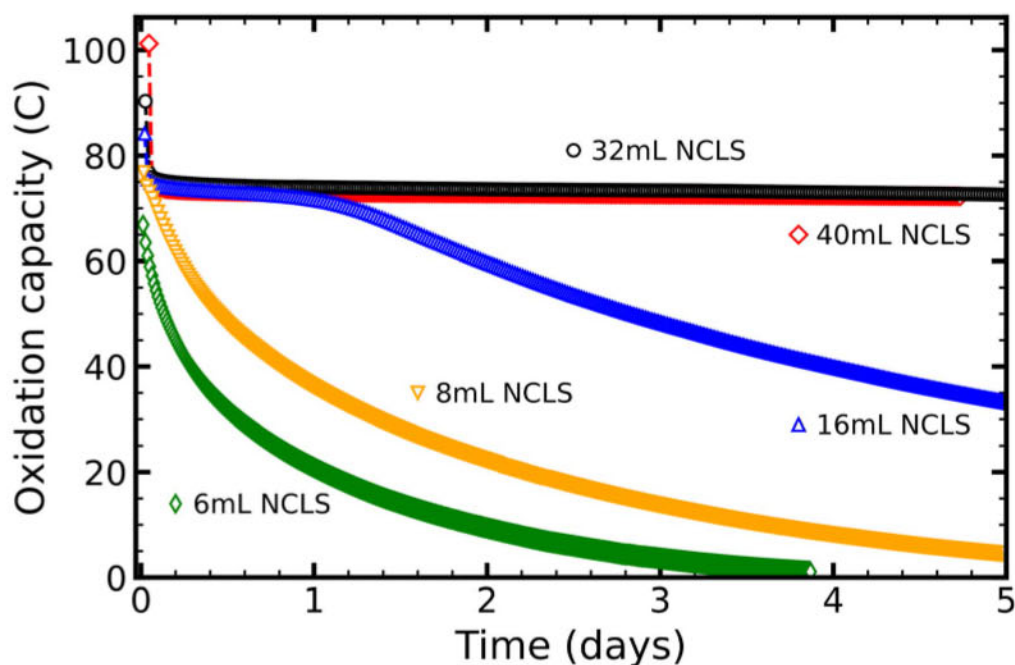


Figure 9. Potentiostatic cycling of 0.1 M ferri-/0.1 M ferrocyanide pH 14 volumetrically unbalanced compositionally symmetric cells with SGL electrodes, 4.0 ml CLS, and varying NCLS volumes.

the apparent capacity fade appears to shift from a regime of precipitous drop (NCLS of 6 ml, 8 ml), to one that takes roughly a day to become unbalanced and rollover (NCLS of 16 ml), and finally to a regime where the cells did not become unbalanced for the duration of cycling (NCLS of 32 ml, 40 ml).

Results that follow the trends of the fixed CLS volume experiments are shown in Fig. 10 where we report the effect of the NCLS:CLS volume ratio on apparent capacity fade. As before, we cycled 0.1 M ferri-/0.1 M ferrocyanide pH 14 electrolytes in cells with SGL electrodes at multiple CLS and NCLS volume configurations, now plotted considering the volume ratio of the two reservoirs and including some data from Figs. 8 & 9. The trends from Fig. 9 still apply, but we can now see a shift with volume ratio of the relationship between apparent capacity fade rate and CLS volume. As the NCLS:CLS volume ratio increases, apparent capacity fade rates decrease for a given CLS volume. A larger NCLS volume provides additional capacity which allows for a full swing in CLS SOC for a longer fraction of the cycling experiment before the NCLS becomes capacity-limiting. Cells with the smallest volume CLS for a fixed NCLS:CLS ratio have the largest ratio of carbon electrode surface area to ferricyanide, thereby accelerating the chemical redox process that leads to rapid unbalancing. By varying CLS and NCLS volumes, and their ratio, we demonstrate that an apparent capacity fade rate in alkaline ferri-/ferrocyanide symmetric cells is essentially an engineered quantity i.e., an apparent fade rate depends on the choice of cell geometry (electrode surface area, volumes of CLS and NCLS, volume ratio of NCLS:CLS) and electrolyte composition (pH, total amount of ferri-/ferrocyanide) and thus any fair comparison of apparent fade rates in ferri-/ferrocyanide symmetric cells must include a description of all such flow battery parameters.

Conditions enabling the practical use of ferri/ferricyanide in AORFBs.—Based on the experiments reported here and those in Refs. 33, 34, 36, 37, we offer the following observations enabling practical utilization of alkaline ferri-/ferrocyanide electrolytes in AORFBs:

- For a 50% SOC electrolyte, the chemical reduction of ferricyanide via chemical OER is thermodynamically unfavorable below pH 11.1 in a glovebox and pH 12.3 in air. However,

given the Nernstian shift in potential as a function of SOC, lower pH electrolytes may still lead to small amounts of chemical ferricyanide reduction/OER at SOC extremes.

- The chemical reduction of ferricyanide can be limited by maintaining high oxygen partial pressure in the reservoir headspace or by sealing the headspace to permit the partial pressure to build during use. However, one must be careful to not simply open the headspace to air containing CO₂, as this would introduce carbonates and decrease the electrolyte pH.
- At pH 14, the electrode-catalyzed apparent capacity fade rate at which ferricyanide converts to ferrocyanide through chemical reduction via OER decreases as the ratio of the total number of ferricyanide ions to the electrode surface area increases. Consequently, we anticipate that this effect should be negligible with the large electrolyte volumes and volumetric capacities required for practical flow battery installations with energy/power ratios of several hours.
- Carbon electrodes with less surface area should be less active in promoting parasitic reduction of ferricyanide. Graphitic binder in certain carbon electrodes may also balance the chemical reduction of ferricyanide via carbon oxidation.
- If parasitic reduction of ferricyanide is unavoidable in a given system architecture, then it may be feasible to use rebalancing techniques such as electrochemical oxidation coupled with hydrogen evolution or the oxygen reduction reaction,⁶⁶ as there is no structural decomposition of the ferri-/ferrocyanide redox-active species.

Conclusions

In the dark or in diffuse indoor light, ferri-/ferrocyanide is structurally stable in alkaline electrolytes of pH up to 14. A pH-dependent chemical reduction of ferricyanide to ferrocyanide, via chemical OER, occurs in alkaline electrolytes. The rate of this chemical redox reaction is enhanced by carbon electrode active surface area and, in some cases, balanced in part by chemical carbon oxidation. Symmetric cell cycling experiments show that apparent capacity fade arises from the chemical redox process, taking the SOC of the CLS and NCLS out of balance, thereby decreasing the accessible capacity of the system. The apparent capacity loss can be completely recovered by refreshing the NCLS or by various

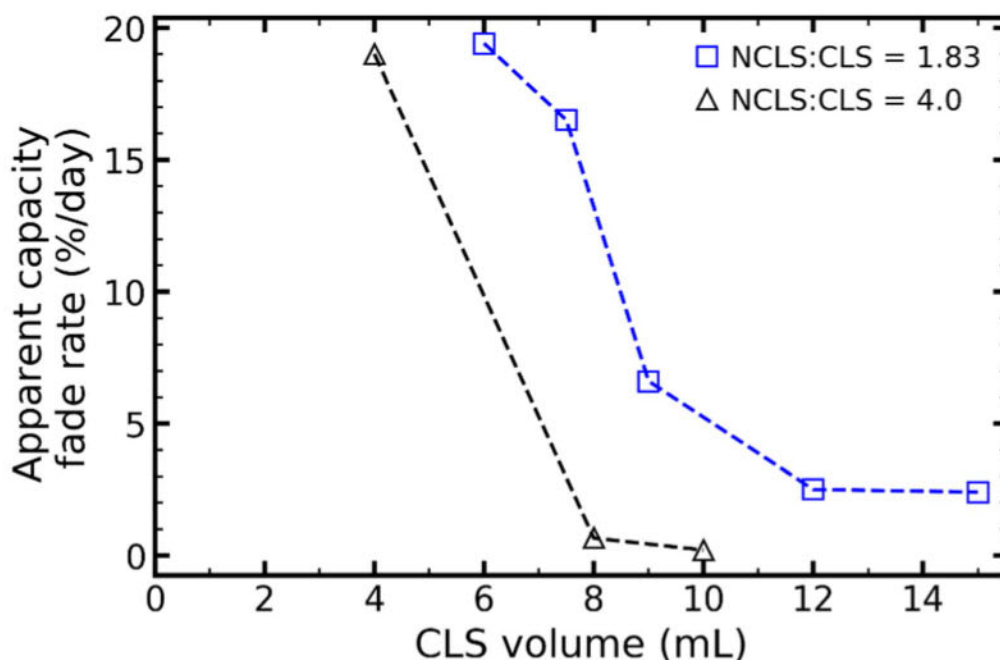


Figure 10. Apparent capacity fade rates of potentiostatically cycled 0.1 M ferri-/0.1 M ferrocyanide pH 14 volumetrically unbalanced compositionally symmetric cells with SGL electrodes and fixed NCLS:CLS volume ratios. Lines are meant only to guide the eye.

rebalancing techniques. We also present evidence to support our arguments that Refs. 33, 37 have incorrectly attributed apparent capacity fade to the chemical degradation of ferri-/ferrocyanide and assigned a carbonate peak to free cyanide. We show that symmetric cell unbalancing occurs due to chemical OER rather than electrochemical OER as previously concluded in Ref. 36. Our experiments further demonstrate that the apparent capacity fade rate at pH 14 decreases as the ratio of the total number of ferricyanide ions to the electrode surface area increases. We reveal how the apparent capacity fade rate of an alkaline ferri-/ferrocyanide symmetric cell may be manipulated by the choice of electrode area, reservoir volumes, pH, and ferri-/ferrocyanide content. Based on these results, we anticipate that, in a commercial scale application with the large electrolyte volumes required for RFB installations with energy/power ratios of several hours, cycling once or twice per day, the impact of electrode-catalyzed parasitic ferricyanide chemical reduction at tested pH values up to 14 should be negligible.

Acknowledgments

This research was supported in part by U.S. DOE award DE-AC05-76RL01830 through PNNL subcontract 535264. EMF was supported by the National Science Foundation through grant CBET-1914543. TYG was supported in part by the National Science Foundation Graduate Research Fellowship Program under Grant No. DGE 1745303. The authors thank Profs. Marc-Antoni Goulet and Michael Marshak, Drs. Kiana Amini and Tatsuhiro Tsukamoto, Dawei Xi, and Jordan Sosa for stimulating discussions. We thank the anonymous reviewers for their insightful comments and suggestions.

ORCID

Eric M. Fell  <https://orcid.org/0000-0003-2046-1480>

Thomas Y. George  <https://orcid.org/0000-0002-0159-8521>

Michael J. Aziz  <https://orcid.org/0000-0001-9657-9456>

References

- B. T. Huskinson, M. P. Marshak, C. Suh, S. Er, M. R. Gerhardt, C. J. Galvin, X. Chen, A. Aspuru-Guzik, R. G. Gordon, and M. J. Aziz, "A metal-free organic-inorganic aqueous flow battery." *Nature*, **505**, 195 (2014).
- K. Lin et al., "Alkaline quinone flow battery." *Sci.*, **349**, 1529 (2015).
- T. Liu, X. Wei, Z. Nie, V. Sprenkle, and W. Wang, "A total organic aqueous redox flow battery employing a low cost and sustainable methyl viologen anolyte and 4-HO-TEMPO catholyte." *Adv. Energy Mater.*, **6**, 1501449 (2015).
- T. Janoschka, N. Martin, M. D. Hager, and U. S. Schubert, "An aqueous redox-flow battery with high capacity and power: the TEMPTMA/MV system." *Angew. Chem. Int. Ed.*, **55**, 14427 (2016).
- J. Luo, B. Hu, C. Debruler, and T. L. Liu, "A Pi-conjugation extended viologen as a two-electron storage anolyte for total organic aqueous redox flow batteries." *Angew. Chem. Int. Ed.*, **57**, 231 (2018).
- Z. Yang, L. Tong, D. P. Tabor, E. S. Beh, M. A. Goulet, D. De Porcellinis, A. Aspuru-Guzik, R. G. Gordon, and M. J. Aziz, "Alkaline benzoquinone aqueous flow battery for large-scale storage of electrical energy." *Adv. Energy Mater.*, **8**, 1702056 (2018).
- B. Hu, Y. Tang, J. Luo, G. Grove, Y. Guo, and T. L. Liu, "Improved radical stability of viologen anolytes in aqueous organic redox flow batteries." *Chem. Commun.*, **54**, 6871 (2018).
- D. G. Kwabi et al., "Alkaline quinone flow battery with long lifetime at pH 12." *Joule*, **2**, 1894 (2018).
- Y. Liu, S. Lu, S. Chen, H. Wang, J. Zhang, and Y. Xiang, "A sustainable redox flow battery with alizarin-based aqueous organic electrolyte." *ACS Appl. Energy Mater.*, **2**, 2469 (2019).
- Y. Ji, M.-A. Goulet, D. A. Pollack, D. G. Kwabi, S. Jin, D. Porcellinis, E. F. Kerr, R. G. Gordon, and M. J. Aziz, "A phosphonate-functionalized quinone redox flow battery at near-neutral pH with record capacity retention rate." *Adv. Energy Mater.*, **9**, 1900039 (2019).
- M.-A. Goulet, L. Tong, D. A. Pollack, D. P. Tabor, S. A. Odom, A. Aspuru-Guzik, E. E. Kwan, R. G. Gordon, and M. J. Aziz, "Extending the lifetime of organic flow batteries via redox state management." *J. Am. Chem. Soc.*, **141**, 8014 (2019).
- S. Jin, Y. Jing, D. G. Kwabi, Y. Ji, L. Tong, D. De Porcellinis, M. A. Goulet, D. A. Pollack, R. G. Gordon, and M. J. Aziz, "A water-miscible quinone flow battery with high volumetric capacity and energy density." *ACS Energy Lett.*, **4**, 1342 (2019).
- D. G. Kwabi, Y. Ji, and M. J. Aziz, "Electrolyte lifetime in aqueous organic redox flow batteries: a critical review." *Chem. Rev.*, **120**, 6467 (2020).
- M. Wu, Y. Jing, A. A. Wong, E. M. Fell, S. Jin, Z. Tang, R. G. Gordon, and M. J. Aziz, "Extremely stable anthraquinone negolytes synthesized from common precursors." *Chem*, **6**, 11 (2020).
- A. Hollas, X. Wei, V. Murugesan, Z. Nie, B. Li, D. Reed, J. Liu, V. Sprenkle, and W. Wang, "A biomimetic high-capacity phenazine-based anolyte for aqueous organic redox flow batteries." *Nat. Energy*, **3**, 508 (2018).
- R. Feng et al., "Reversible ketone hydrogenation and dehydrogenation for aqueous organic redox flow batteries." *Sci.*, **372**, 836 (2021).
- J. Xu, S. Pang, X. Wang, P. Wang, and Y. Ji, "Ultrastable aqueous phenazine flow batteries with high capacity operated at elevated temperatures." *Joule*, **5**, 2437 (2021).
- G. B. Adams, R. P. Hollandsworth, and B. D. Webber, *Rechargeable Alkaline Zinc/Ferricyanide Battery: Final Report for the Period 29 September 1978-28 September 1979* (Lockheed Palo Alto Research Laboratory, Lockheed Missiles & Space Co., Palo Alto, Calif.) (1979).
- T. Janoschka, N. Martin, U. Martin, C. Friebe, S. Morgenstern, H. Hiller, M. D. Hager, and U. S. Schubert, "An aqueous, polymer-based redox-flow battery using non-corrosive, safe, and low-cost materials." *Nature*, **527**, 78 (2015).
- K. Wedege, E. Drazevic, D. Konya, and A. Bienten, "Organic redox species in aqueous flow batteries: redox potentials, chemical stability and solubility." *Sci. Rep.*, **6**, 39101 (2016).
- E. S. Beh, D. De Porcellinis, R. L. Gracia, K. T. Xia, R. G. Gordon, and M. J. Aziz, "A neutral pH aqueous organic-organometallic redox flow battery with extremely high capacity retention." *ACS Energy Lett.*, **2**, 639 (2017).
- E. Drazevic, C. Szabo, D. Konya, T. Lund, K. Wedege, and A. Bienten, "Investigation of tetramorpholinohydroquinone as a potential catholyte in a flow battery." *ACS Appl. Energy Mater.*, **2**, 4745 (2019).
- M. Park et al., "A high voltage aqueous zinc-organic hybrid flow battery." *Adv. Energy Mater.*, **9**, 1900694 (2019).
- W. Ruan, J. Mao, S. Yang, and Q. Chen, "Communication—Tris(Bipyridyl)iron complexes for high-voltage aqueous redox flow batteries." *J. Electrochem. Soc.*, **167**, 100543 (2020).
- X. Li et al., "Symmetry-breaking design of an organic iron complex catholyte for a long cyclability aqueous organic redox flow battery." *Nat. Energy*, **6**, 873 (2021).
- J. Gao, K. Amini, T. Y. George, Y. Jing, T. Tsukamoto, D. Xi, R. G. Gordon, and M. J. Aziz, "A high potential, low capacity fade rate iron complex polysolite for aqueous organic flow batteries." *Adv. Energy Mater.*, **12**, 2202444 (2022).
- F. R. Brushett, M. J. Aziz, and K. E. Rodby, "On lifetime and cost of redox-active organics for aqueous flow batteries." *ACS Energy Lett.*, **5**, 879 (2020).
- Y. Jing et al., "In situ electrochemical recombination of decomposed redox-active species in aqueous organic flow batteries." *Nat. Chem.*, **14**, 1103 (2022).
- J. Preusz, "Vermischte chemische notizen." *Annalen der Pharmacie*, **29**, 323 (1839).
- S. Ašperger, "Kinetics of the decomposition of potassium ferrocyanide in ultra-violet light." *Trans. Faraday Soc.*, **48**, 617 (1952).
- C. A. P. Arellano and S. S. Martinez, "Effects of pH on the degradation of aqueous ferricyanide by photolysis and photocatalysis under solar radiation." *Sol. Energy Mater. Sol. Cells*, **94**, 327 (2010).
- M. Reinhard, T. J. Penfold, F. A. Lima, J. Rittmann, M. H. Rittmann-Frank, R. Abela, I. Tavernelli, U. Rothlisberger, C. J. Milne, and M. Chergui, "Photooxidation and photoaquation of iron hexacyanide in aqueous solution: a picosecond X-ray absorption study." *Structural Dynamics*, **1**, 024901 (2014).
- J. Luo, A. Sam, B. Hu, C. DeBruler, X. Wei, W. Wang, and T. L. Liu, "Unraveling pH dependent cycling stability of ferricyanide/ferrocyanide in redox flow batteries." *Nano Energy*, **42**, 215 (2017).
- M.-A. Goulet and M. J. Aziz, "Flow battery molecular reactant stability determined by symmetric cell cycling methods." *J. Electrochem. Soc.*, **165**, A1466 (2018).
- M. Cazot, G. Maranzana, J. Dillet, F. Beille, T. Godet-Bar, and S. Didierjean, "Symmetric-cell characterization of the redox flow battery system: application to the detection of degradations." *Electrochim. Acta*, **321**, 134705 (2019).
- T. Páez, A. Martínez-Cuevas, J. Palma, and E. Ventosa, "Revisiting the cycling stability of ferrocyanide in alkaline media for redox flow batteries." *J. Power Sources*, **471**, 228453 (2020).
- M. Hu, A. P. Wang, J. Luo, Q. Wei, and T. L. Liu, "Cycling performance and mechanistic insights of ferricyanide electrolytes in alkaline redox flow batteries." *Advanced Energy Materials*, **13**, 2203762 (2023).
- J. D. Benck, B. A. Pinaud, Y. Gorlin, and T. F. Jaramillo, "Substrate selection for fundamental studies of electrocatalysts and photoelectrodes: inert potential windows in acidic, neutral, and basic electrolyte." *PLoS One*, **9**, e107942 (2014).
- J. Luo, B. Hu, C. Debruler, Y. Bi, Y. Zhao, B. Yuan, M. Hu, W. Wu, and T. L. Liu, "Unprecedented capacity and stability of ammonium ferrocyanide catholyte in pH neutral aqueous redox flow batteries." *Joule*, **3**, 149 (2019).
- S. V. Grayly, X. Zhang, F. C. MacNab, S. Kamal, D. Star, and G. W. Leach, "Scalable, green fabrication of single-crystal noble metal films and nanostructures for low-loss nanotechnology applications." *ACS Nano*, **14**, 7581 (2020).
- M. Bogdanov, R. Gryboš, and A. Samotus, "Electron-transfer kinetics and mechanism of the reduction of octacyanometallates(IV) (M=Mo, W) by hydroxide ion in aqueous solution." *Transition Met. Chem.*, **18**, 599 (1993).
- J. Feeney, A. S. V. Burgen, and E. Grell, "Cyanide binding to carbonic anhydrase." *Eur. J. Biochem.*, **34**, 107 (1973).
- J. Seravalli and S. W. Ragsdale, "13C NMR characterization of an exchange reaction between CO and CO2 catalyzed by carbon monoxide dehydrogenase." *Biochemistry*, **47**, 6770 (2008).
- T. M. Abbott, G. W. Buchanan, P. Kruus, and K. C. Lee, "13C nuclear magnetic resonance and raman investigations of aqueous carbon dioxide systems." *Can. J. Chem.*, **60**, 1000 (1982).
- F. Mani, M. Peruzzini, and P. Stoppioni, "CO2 absorption by aqueous NH3 solutions: speciation of ammonium carbamate, bicarbonate and carbonate by a 13C NMR study." *Green Chem.*, **8**, 995 (2006).

46. M. Shin, C. Noh, Y. Chung, and Y. Kwon, "All iron aqueous redox flow batteries using organometallic complexes consisting of iron and 3-[Bis (2-Hydroxyethyl) Amino]-2-hydroxypropanesulfonic acid ligand and ferrocyanide as redox couple." *Chem. Eng. J.*, **398**, 125631 (2020).
47. C. Bleasdale, B. T. Golding, J. McGinnis, S. Müller, and W. P. Watson, "The mechanism of decomposition of *N*-Methyl-*N*-nitrosourea in aqueous solution according to ¹³C and ¹⁵N NMR studies: quantitative fragmentation to cyanate." *J. Chem. Soc., Chem. Commun.*, **24**, 1726 (1991).
48. J. S. Silvia and C. C. Cummins, "Two-electron reduction of a vanadium(V) nitride by CO to release cyanate and open a coordination site." *J. Am. Chem. Soc.*, **131**, 446 (2009).
49. V. K. Kriehle and J. G. McNally, "The hydrolysis of hydrogen cyanide by acids." *J. Am. Chem. Soc.*, **51**, 3368 (1929).
50. V. K. Kriehle and A. L. Peiker, "The hydrolysis of hydrogen cyanide by acids. II." *J. Am. Chem. Soc.*, **55**, 2326 (1933).
51. J. D. F. Marsh and M. J. Martin, "The hydrolysis and polymerization of hydrogen cyanide in alkaline solutions." *J. Appl. Chem.*, **7**, 205 (1957).
52. E. Gail, S. Gos, R. Kulzer, J. Lorösch, A. Rubo, M. Sauer, R. Kellens, J. Reddy, N. Steier, and W. Hasenpusch, "Cyano compounds, inorganic." *Ullmann's Encyclopedia of Industrial Chemistry* (2011).
53. S. E. Waters, B. H. Robb, S. J. Scappaticci, J. D. Saraidaridis, and M. P. Marshak, "Isolation and characterization of a highly reducing aqueous chromium(II) complex." *Inorg. Chem.*, **61**, 8752 (2022).
54. B. H. Robb, J. M. Farrell, and M. P. Marshak, "Chelated chromium electrolyte enabling high-voltage aqueous flow batteries." *Joule*, **3**, 2503 (2019).
55. K. V. Greco, A. Forner-Cuenca, A. Mularczyk, J. Eller, and F. R. Brushett, "Elucidating the nuanced effects of thermal pretreatment on carbon paper electrodes for vanadium redox flow batteries." *ACS Appl. Mater. Interfaces*, **10**, 44430 (2018).
56. A. Forner-Cuenca, E. E. Penn, A. M. Oliveira, and F. R. Brushett, "Exploring the role of electrode microstructure on the performance of non-aqueous redox flow batteries." *J. Electrochem. Soc.*, **166**, A2230 (2019).
57. A. A. Wong and M. J. Aziz, "Method for comparing porous carbon electrode performance in redox flow batteries." *J. Electrochem. Soc.*, **167**, 110542 (2020).
58. D. Zhang, A. Forner-Cuenca, O. O. Taiwo, V. Yufit, F. R. Brushett, N. P. Brandon, S. Gu, and Q. Cai, "Understanding the role of the porous electrode microstructure in redox flow battery performance using an experimentally validated 3D pore-scale lattice boltzmann model." *J. Power Sources*, **447**, 227249 (2020).
59. K. M. Tenny, A. Forner-Cuenca, Y.-M. Chiang, and F. R. Brushett, "Comparing physical and electrochemical properties of different weave patterns for carbon cloth electrodes in redox flow batteries." *Journal of Electrochemical Energy Conversion and Storage*, **17**, 041010 (2020).
60. K. M. Tenny, K. V. Greco, M. van der Heijden, T. Pini, A. Mularczyk, A.-P. Vasile, J. Eller, A. Forner-Cuenca, Y.-M. Chiang, and F. R. Brushett, "A comparative study of compressive effects on the morphology and performance of carbon paper and cloth electrodes in redox flow batteries." *Energy Technology*, **10**, 2101162 (2022).
61. M. H. Chakrabarti, N. P. Brandon, S. A. Hajimolana, F. Tariq, V. Yufit, M. A. Hashim, M. A. Hussain, C. T. J. Low, and P. V. Aravind, "Application of carbon materials in redox flow batteries." *J. Power Sources*, **253**, 150 (2014).
62. S. Dussi and C. H. Rycroft, "Less can be more: insights on the role of electrode microstructure in redox flow batteries from two-dimensional direct numerical simulations." *Phys. Fluids*, **34**, 04311 (2022).
63. J. Luo, A. P. Wang, M. Hu, and T. L. Liu, "Materials challenges of aqueous redox flow batteries." *MRS Energy & Sustainability*, **9**, 1 (2022).
64. Z. Yuan, Y. Duan, T. Liu, H. Zhang, and X. Li, "Toward a low-cost alkaline zinc-iron flow battery with a polybenzimidazole custom membrane for stationary energy storage." *iScience*, **3**, 40 (2018).
65. Y. Jing, M. Wu, A. A. Wong, E. M. Fell, S. Jin, D. A. Pollack, E. F. Kerr, R. G. Gordon, and M. J. Aziz, "In situ electrosynthesis of anthraquinone electrolytes in aqueous flow batteries." *Green Chem.*, **22**, 6084 (2020).
66. T. Páez, A. Martínez-Cuezva, R. Marcilla, J. Palma, and E. Ventosa, "Mitigating capacity fading in aqueous organic redox flow batteries through a simple electrochemical charge balancing protocol." *J. Power Sources*, **512**, 230516 (2021).

Long-term Stability of Ferri-/Ferrocyanide as an Electroactive Component for Redox Flow Battery Applications: On the Origin of Apparent Capacity Fade

Supporting Information

Eric M. Fell^{1,*}, Diana De Porcellinis¹, Yan Jing², Valeria Gutierrez-Venegas³, Thomas Y. George^{1,*}, Roy G. Gordon², Sergio Granados-Focil³, Michael J. Aziz^{1,z,**}

¹ Harvard John A. Paulson School of School of Engineering and Applied Sciences, 29 Oxford Street, Cambridge, MA, 02138, USA.

² Department of Chemistry and Chemical Biology, Harvard University, 12 Oxford Street, Cambridge, MA, 02138, USA.

³ Gustaf Carlson School of Chemistry and Biochemistry, Clark University, Worcester, MA, 01610-1477, USA

^zCorresponding Author Information:

Prof. Michael J. Aziz,

Address: Harvard John A. Paulson School of Engineering and Applied Sciences, 29 Oxford Street, Cambridge, Massachusetts 02138, USA

Email: maziz@harvard.edu

Tel: (617) 495-9884,

Fax: (617) 495-9837

*ECS Student Member; **ECS Member

Contents

Figure S1. Schematic of temporal evolution of capacity and ferricyanide fractions in CLS/NCLS.....	3
Figure S2. Extended view of ^{13}C NMR spectra shown in Figure 3 of main text	4
Figure S3. ^1H NMR spectra of ferrocyanide solutions with electrodes	5
Figure S4. UV-Vis of high concentration ferricyanide solutions.....	6
Figure S5. Pictures of ferricyanide solutions kept in light/dark.....	7
Figure S6. UV-Vis of ferricyanide solutions in polypropylene vials.....	8
Figure S7. GC traces for ferricyanide solutions.....	9
Figure S8. MS spectra for ferricyanide solutions.....	10
Table S1. Decrease in hydroxide concentrations, shown in Figure 6 of main text	12
Figure S9. UV-Vis of ferricyanide solutions in glass vials, HCBA electrodes.....	11
Table S2. BET surface area measurements	12
Figure S10. SEM images of electrodes	12
Figure S11. EDS analysis of SGL electrode	13
Figure S12. EDS analysis of HCBA electrode.....	13
Figure S13. Pictures of cycled electrolytes	14
Figure S14. CLS refresh experiment, low concentration ferri-/ferrocyanide.....	14

Supplementary Information

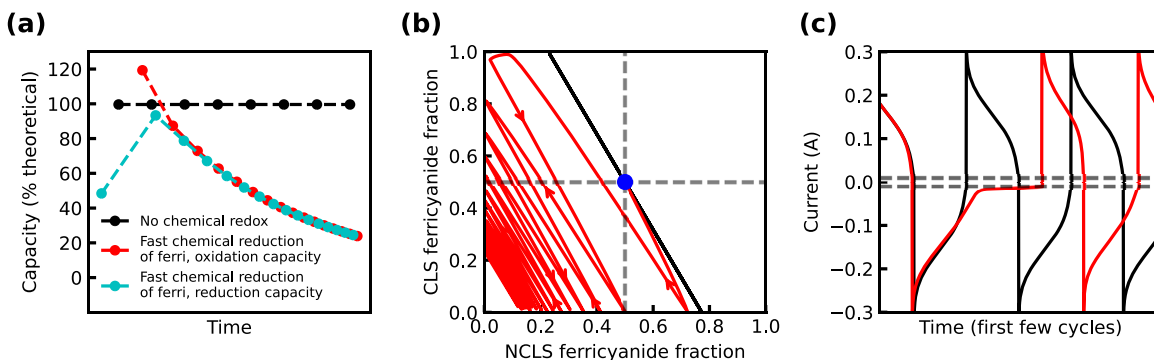


Figure S1. Idealized schematic of two ferri-/ferrocyanide volumetrically unbalanced compositionally symmetric cells cycled potentiostatically, one without chemical reduction of ferricyanide (e.g., pH 7) and one exhibiting fast chemical reduction of ferricyanide (e.g., pH 14), with an NCLS volume double that of the CLS. (a) CLS oxidation capacity, normalized to theoretical capacity, of individual cycles over time; (b) Trace of temporal evolution of accessed ferricyanide fractions in CLS/NCLS reservoirs during the cycles shown in (a). The blue circle indicates the starting point for both cells i.e., 50% SOC in the CLS and NCLS. Gray dashed lines indicate ferricyanide fractions of 0.5; (c) Current profiles of the first few charge/discharge (reduction/oxidation of CLS) cycles shown in (a). Gray dashed lines indicate ± 10 mA current cutoffs.

A schematic of cell cycling behavior as a function of the rate of chemical reduction of ferricyanide is shown in **Fig. S1**. Both idealized cells begin by potentiostatically charging the CLS (ferricyanide electrochemically reduced to ferrocyanide in CLS, ferrocyanide electrochemically oxidized to ferricyanide in NCLS). For the cell exhibiting fast chemical reduction of ferricyanide (red), the temporal trace of SOC evolution in (b) demonstrates continual slippage in ferricyanide fractions due to the chemical redox process occurring in both reservoirs. The black trace in (b) for the cell without chemical reduction of ferricyanide overlays itself for every cycle because there is no slippage in ferricyanide fractions in either reservoir. It should be noted that the axes of (b) are not scaled to the actual volumes of the CLS/NCLS. Curvature of the red SOC trace during the first oxidation (discharge) cycle (top left corner of (b)), and the resulting precipitous drop in apparent capacity seen in (a), are further explained by the current profiles in (c): The first oxidation (negative current) for the red trace shows a low current plateau for some extended time before finally hitting the current cutoff and switching to reduction. During this current plateau, the CLS is almost fully oxidized (ferricyanide) but chemical reduction of ferricyanide to ferrocyanide still occurs, allowing for continued electrochemical oxidation of regenerated ferrocyanide at oxidation currents with absolute values greater than oxidation current cutoff limits. This explains why the cell exhibiting a fast chemical reduction rate of ferricyanide demonstrates an initial oxidation cycle achieving greater than 100% theoretical capacity (similar to the SGL pH 14 cells of **Figs. 1&9**). Meanwhile, the excess CLS oxidation capacity must be balanced by available capacity in the

NCLS i.e., electrochemical reduction of ferricyanide in the NCLS, shifting the NCLS ferricyanide fraction to the left in (b). Once the NCLS hits a ferricyanide fraction of zero, it becomes capacity-limiting and the measured cell capacity will continue to drop over time because not all available capacity in the CLS can be charged/discharged. It should also be noted that the act of refreshing the NCLS with a new 50% SOC electrolyte (**Figs. 7&S14**) shifts the SOC trace in (b) to the right, to a NCLS ferricyanide fraction of 0.5, if it has moved from the ideal situation (black). The act of refreshing the CLS with a new 50% SOC electrolyte shifts the trace upward to a CLS ferricyanide fraction of 0.5.

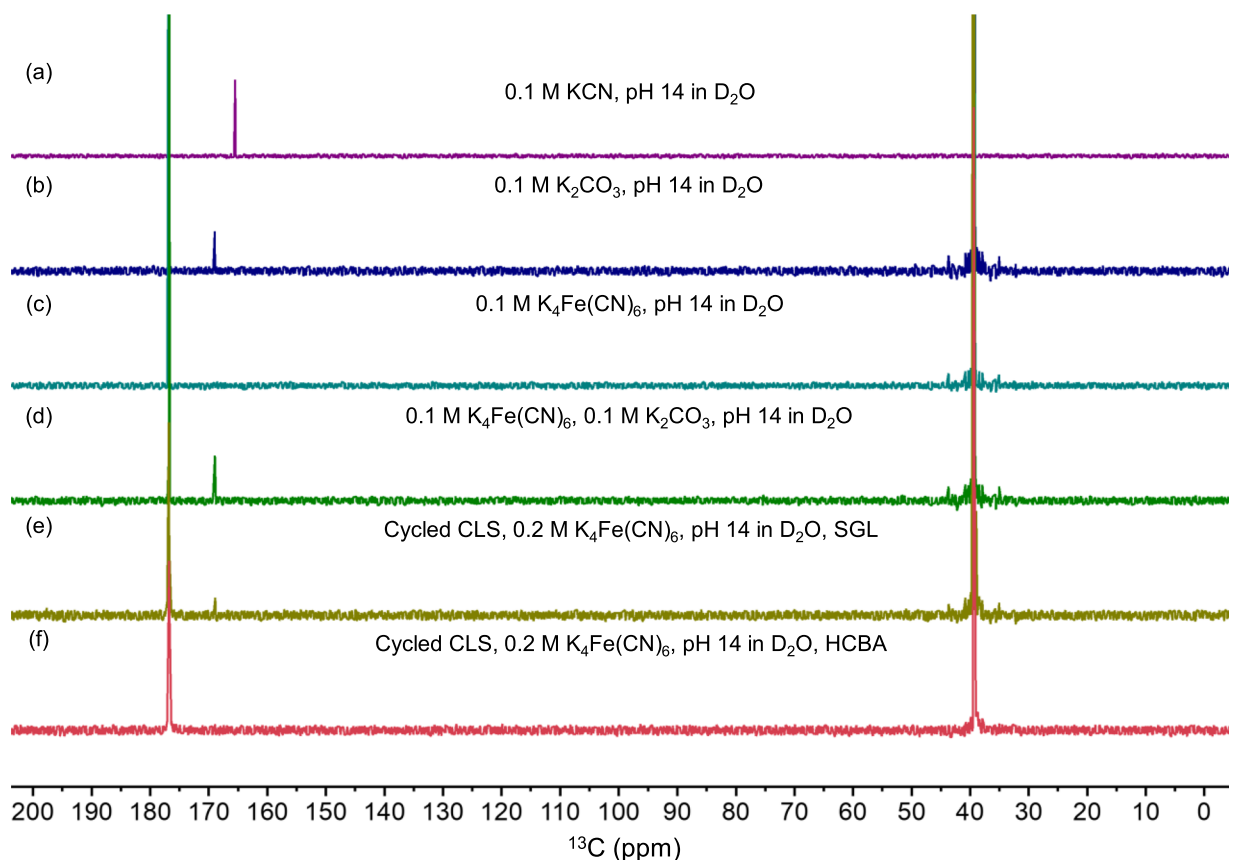


Figure S2. Extended view of ¹³C NMR spectra shown in Figure 3 of main text, now showing the DMSO internal standard in each sample located at 39 ppm.

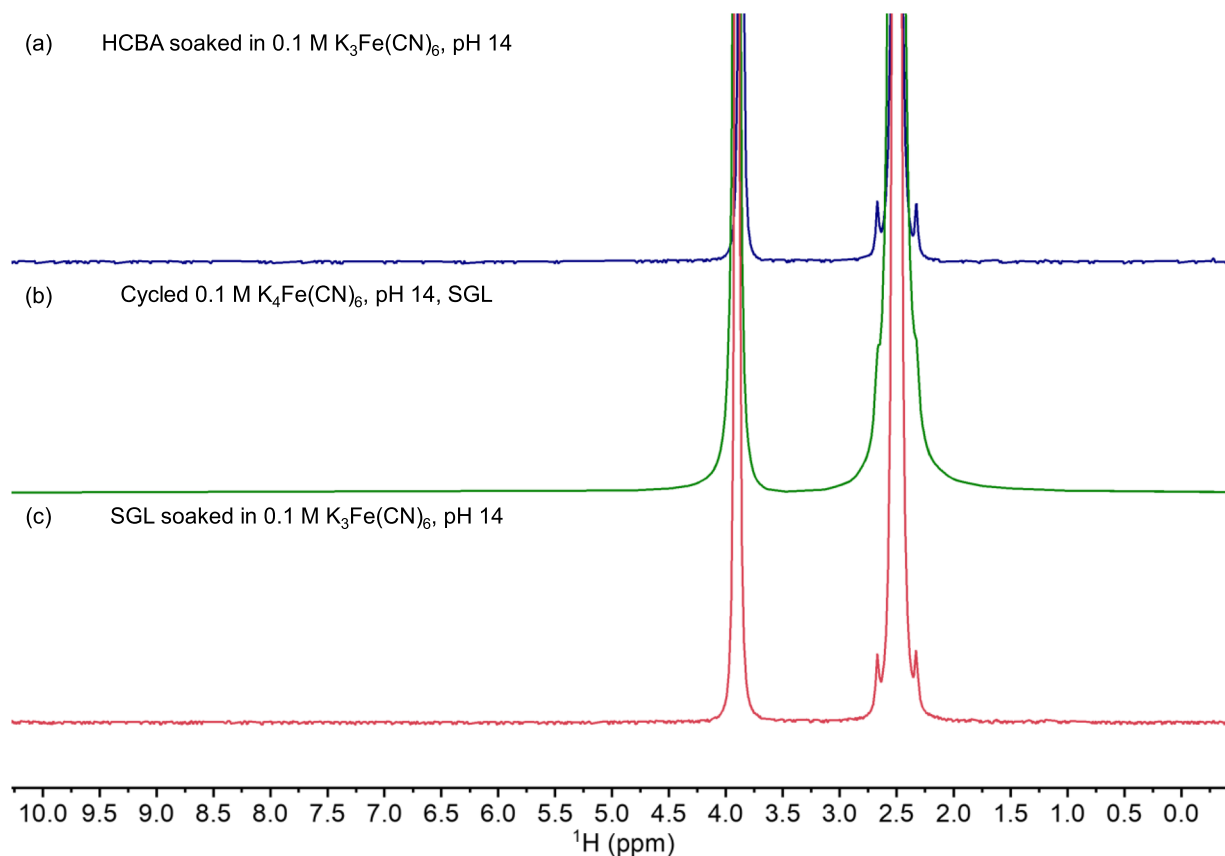


Figure S3. ^1H NMR measurements of samples from electrolyte of 0.1 M ferricyanide pH 14 left soaking (a) an HCBA electrode, and (c) an SGL electrode, after six months of soaking. (b) Cycled CLS (electrochemically reduced to ferrocyanide) of 0.1 M ferri-/0.1 M ferrocyanide pH 14 symmetric cell with SGL electrodes, after seven days of cycling. All samples were kept in glovebox in the dark until removed for NMR measurement, at which point 100 μL of electrolyte was added to 550 μL of DMSO-d_6 solvent (peak at 2.5 ppm). The peak at 3.9 ppm is from the H_2O in the ferri-/ferrocyanide electrolytes. No ammonia was detected (the expected triplet peak would occur at 7 ppm).

We investigated the rate of chemical reduction in higher concentration ferricyanide electrolytes at pH 14, in the absence of electrodes. First, three replicates of 50 mL of 0.1 M ferricyanide at pH 14, and three replicates of 50 mL of 0.2 M ferricyanide at pH 14, were made in air. Over 45 days, all samples were kept in the dark (in air), stirred continuously, and kept sealed except when aliquots were removed and diluted for UV-Vis measurements, as shown in **Fig. S4**. In order to mitigate errors in the measured concentration of total iron or ferricyanide from the dilution needed for clear UV-vis spectra, we plot ferricyanide concentration divided by total measured iron concentration. Taking this ratio removes dilution error, which has the same effect on both ferricyanide and total iron for a given individual measurement. We measure instantaneous

chemical reduction rates of $0.023 \pm 0.006\%/day$ and $0.017 \pm 0.004\%/day$ for the 0.1 M ferricyanide and 0.2 M ferricyanide electrolytes, respectively.

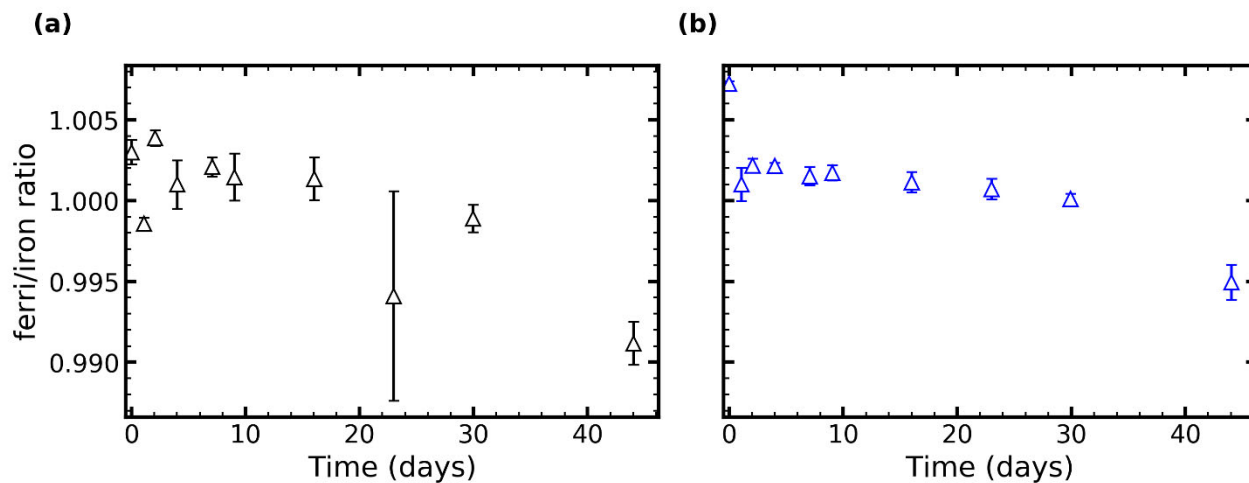


Figure S4. UV-Vis measured time-dependence of ferricyanide, normalized by measured total iron concentration, in 50 mL of pH 14 solution with (a) 0.1 M ferricyanide, or (b) 0.2 M ferricyanide. All samples were stored in oxygen-permeable polypropylene vials and kept in the dark. Error bars indicate standard deviation of three replicates.

After completion of the UV-Vis experiment, all samples were stored for another 50 days either still in the dark or brought out into lab light. **Fig. S5** shows the effect of lab light on precipitate formation.

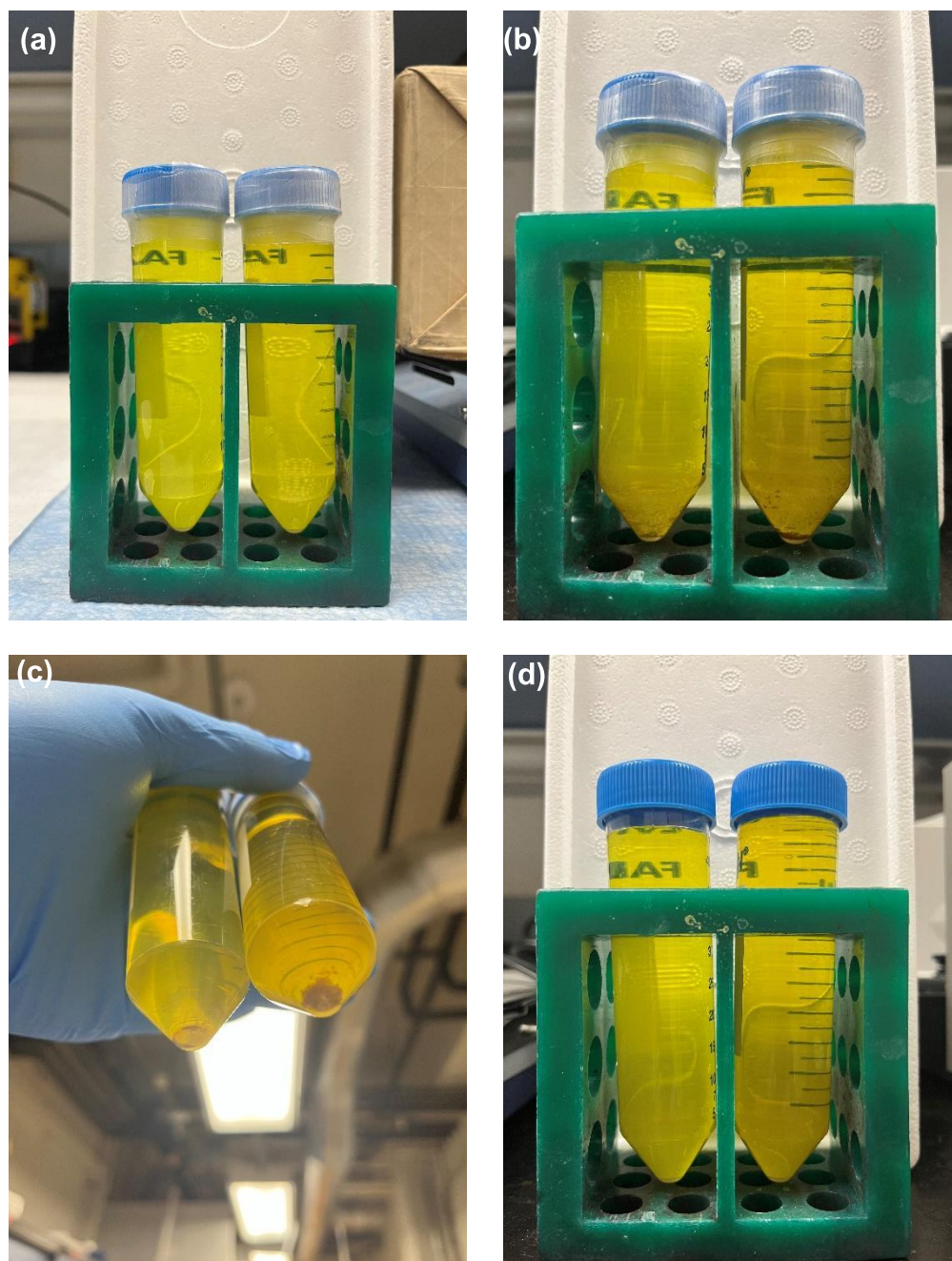


Figure S5. pH 14 ferricyanide electrolytes from the UV-Vis experiments of Fig. S4. In each picture, 0.1 M ferricyanide is on the left and 0.2 M ferricyanide is on the right. (a) Electrolytes after 45 days in the dark (during which, aliquots were taken for data of Fig. S4); (b,c) Electrolytes from (a) subsequently kept in lab light for 50 days. (c) provides another view of the samples in (b) to show rust-colored precipitates in both vials, with more precipitate observed in the 0.2 M ferricyanide electrolyte; (d) Electrolytes from the same initial batch originally kept in the dark for 45 days while performing UV-Vis experiments, subsequently kept in the dark for an additional 50 days with no precipitates observed. Samples came from the same initial respective batches, so that one set could be kept in the dark while the other could be kept in the light.

In an identical experiment to **Fig. 4** of the main text, we used UV-Vis spectrophotometry to measure total ferricyanide and total iron concentrations over time in quiescent solutions with and without carbon electrodes, stored in polypropylene vials, shown in **Fig. S6**. Polypropylene is more oxygen-permeable than glass, therefore as the sealed headspace oxygen partial pressure increases due to the electroless ferricyanide reduction via OER, oxygen can more readily escape the vials, allowing for increased rate of the electroless reaction.

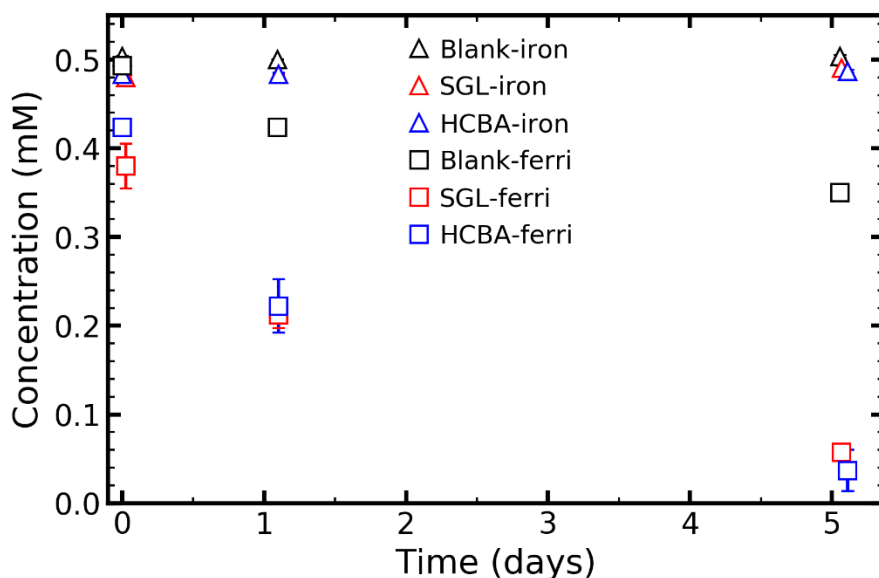


Figure S6. UV-Vis measured time-dependence of ferricyanide and total iron concentration in 3 mL of 0.5 mM ferricyanide pH 14 solution in contact with 4 mm × 4 mm SGL electrode, 4 mm × 4 mm HCBA electrode, or no electrode. All samples were stored in oxygen-permeable polypropylene vials.

Gas chromatography mass-spectrometry (GC-MS) was used to detect the formation of oxygen from solutions of alkaline ferricyanide electrolytes. Three samples were prepared in glovebox: (a) 5 mL of 1 M KOH; (b) 5 mL of 0.25 M ferricyanide in 1 M KOH; (c) 5 mL of 0.25 M ferricyanide in 1 M KOH soaking a 5 cm² SGL carbon electrode. All solutions were sealed in 10 mL air-tight headspace vials for GC-MS measurements. **Fig. S7** shows that an oxygen signal with a retention time of 0.95 minutes was detected from both sample (b) and (c), suggesting that hydroxide ions are indeed oxidized to O₂ while ferricyanide is reduced to ferrocyanide. Furthermore, a stronger oxygen signal (higher signal/noise ratio) is detected from sample (c), implying that the carbon electrode plays a role in this chemical redox reaction. Mass spectroscopy of the GC signal at the retention of 0.95 minutes from GC is shown in **Fig. S8** (top) and the theoretical isotopic pattern of O₂ (bottom).

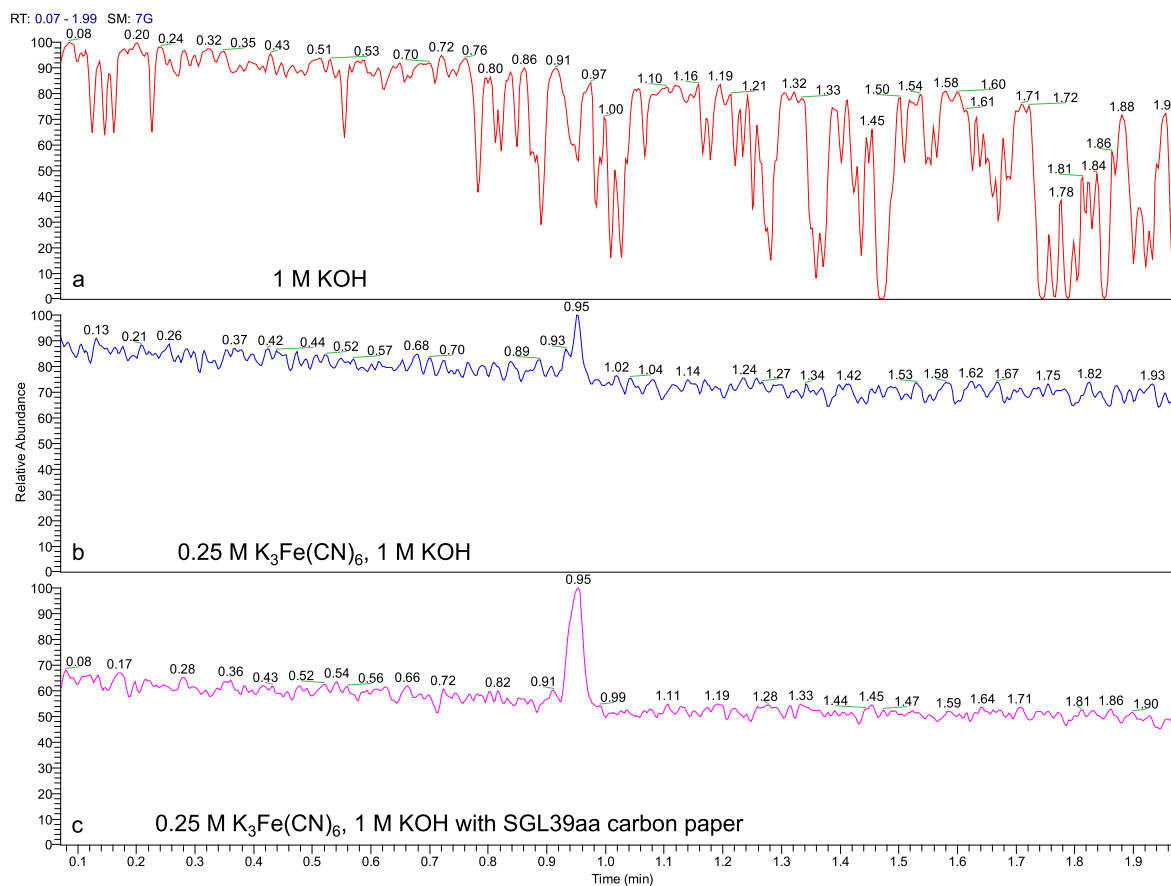


Figure S7. Oxygen detection from gas chromatography (GC) for ferricyanide alkaline solutions. (a) blank sample: 1 M KOH; (b) 0.25 M $K_3Fe(CN)_6$, 1 M KOH; (c) 0.25 M $K_3Fe(CN)_6$, 1 M KOH soaking a 5 cm² baked SGL carbon electrode.

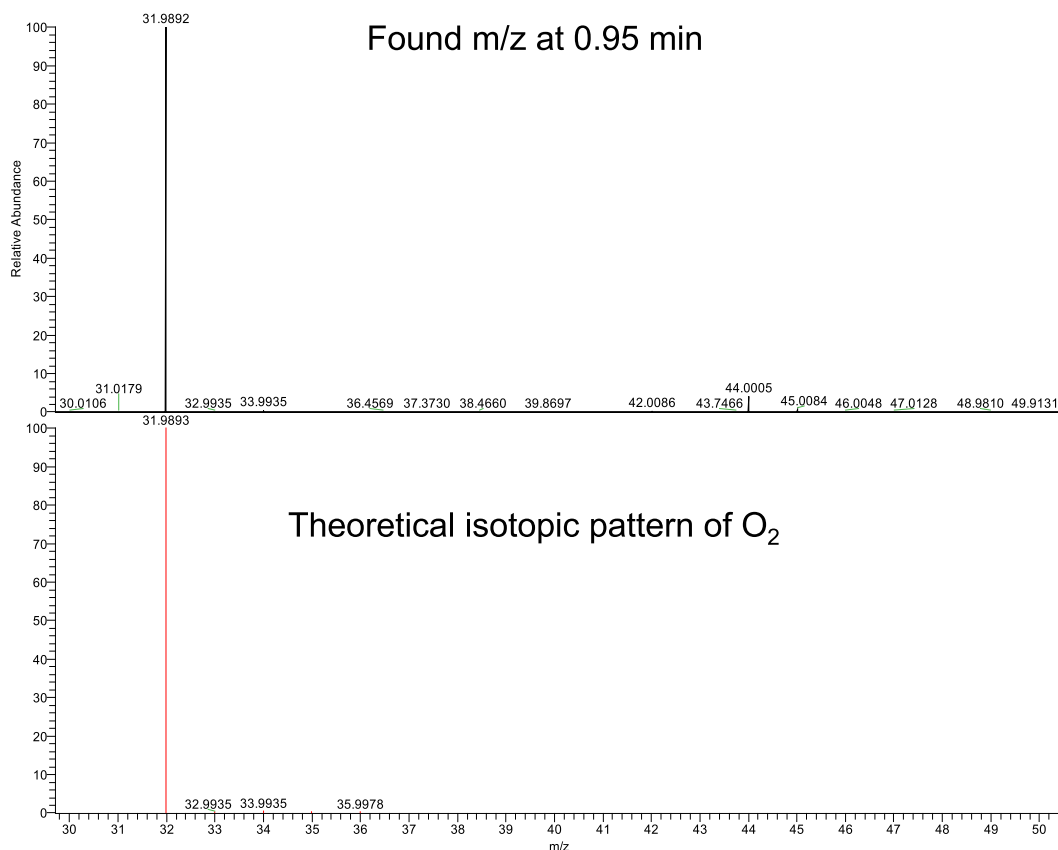


Figure S8. Mass spectroscopy of the gas chromatography signal at retention time of 0.95 minutes (top) and the theoretical isotopic pattern of O₂ (bottom).

GC-MS test conditions

Headspace GC-MS was used for the detection of O₂. The headspace extraction was carried out at 45 °C under agitation on an autosampler (Thermo Scientific TriPlus RSH) for 0.2 min. Then, 40 µL of the headspace sample was injected into the GC-MS system (Thermo Scientific TRACE 1310 Gas Chromatograph). A Thermo fused-silica capillary column of cross-linked TG-5SILMS (30 m x 0.25 mm x 0.25 µm) was used. The GC conditions were as follows: inlet and transfer line temperatures, 120 °C; oven temperature program, 50 °C for 2 min; inlet helium carrier gas flow rate, 1 mL/min; split ratio, 10:1. The electron impact (EI)-MS conditions were as follows: ion source temperature, 250 °C; SIM scan m/z range, 30 – 50 Da; resolution, 60,000; AGC target, 1e6; maximum IT, 200 ms. A mass window of ± 5 ppm was used to extract the pseudomolecular ions of m/z 31.9893 for the detection of O₂. The headspace vials were purchased from Sigma Aldrich. Headspace vial, screw top, rounded bottom, volume 10 mL, clear glass vial, thread for 18, O.D. × H 22.5 mm × 46 mm. Magnetic screw cap for headspace vials, 18 mm thread, PTFE-faced butyl septum (grey PTFE/red Butyl), septum thickness 1.6 mm.

Table S1. Decrease in hydroxide concentrations, from Figure 6 of main text.

pH	SGL	HCBA	No electrode
14	0.199 ± 0.02 M	0.133 ± 0.02 M	0.029 ± 0.02 M
13	0.057 ± 0.002 M	0.015 ± 0.002 M	0.002 ± 0.002 M
12	0.008 ± 0.0002 M	0.005 ± 0.0002 M	0.002 ± 0.0002 M

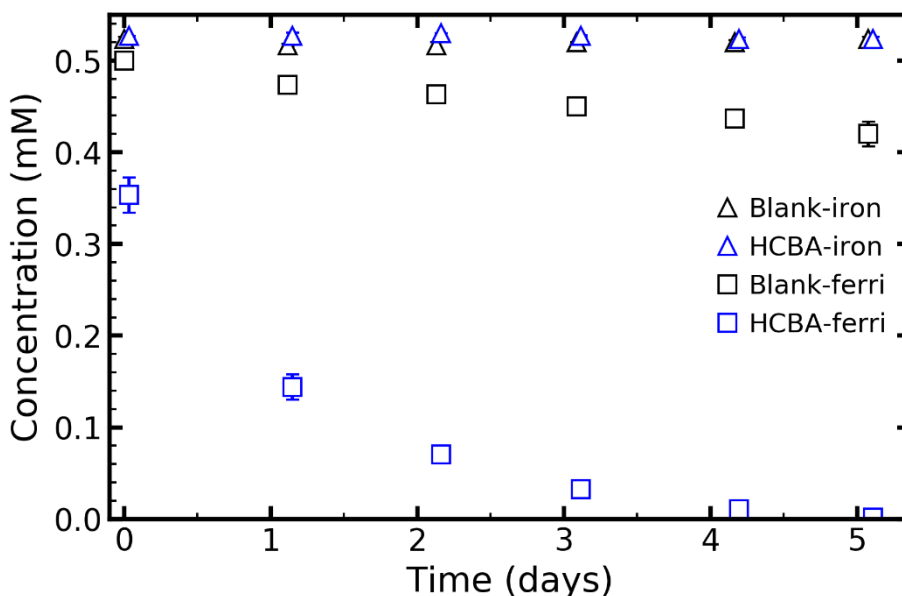


Figure S9. UV-Vis measured time-dependence of ferricyanide and total iron concentration in 3 mL of 0.5 mM ferricyanide pH 14 solution in contact and out of contact with 4 mm \times 4 mm HCBA electrodes. All samples were kept in glass vials.

Physical characterization

The surface area, pore size distribution and total pore volume of the samples were measured by nitrogen adsorption at 77.3 K with a relative pressure P/P_0 from 0.05 to 0.99 using a NOVA 2200e surface area & pore size analyzer (Quantachrome Instruments). All samples were degassed at 250 °C for 3 hours before measurement. Ultra-high purity nitrogen (99.99%) (Middlesex gases & Technologies Inc.) was used as adsorbate for the analysis. The surface area was obtained from the adsorption isotherm data ($0.05 < P/P_0 < 0.3$) using the multi-point Brunauer-Emmet-Teller (BET) method. The pore size distribution was obtained by non-local density functional theory (NLDFT) using the standard slit-pore model for N_2 adsorption at 77 K on carbon. The total pore volume was measured using a single point adsorption at $P/P_0 \sim 0.99$. Specific surface areas of SGL and HCBA electrodes are reported in **Table S2**.

Table S2. BET surface area measurement for SGL and HCBA

electrode	specific area (BET) [m ² /g]	Mass per 5 cm ² sheet [g]	Surface area per electrode [m ²]
SGL	210	0.025	5.3
HCBA	38	0.230	8.7

Scanning Electron Microscopy (SEM) images were acquired using a Hitachi TM-3000 scanning electron microscope equipped with a Back-Scattered Electrons (BSE) detector using a 5 kV acceleration voltage. Energy Dispersive X-Ray Spectroscopy (EDS) measurements were carried out using an energy dispersive spectrometer (Bruker Quantax 50) attached to a Hitachi TM-3000 scanning electron microscope. The EDS spectrometer was calibrated with a copper standard prior to use. All samples were dried under vacuum at 50 °C for 12 hours prior to the measurements. The acceleration voltage in the SEM was 10 kV (analysis mode) and the spectrum acquisition time for all samples was 100 seconds. The sampling area was approximately 3 mm. SEM images of SGL and HCBA electrodes are shown in **Fig. S10**. EDS spectra are shown in **Figs. S11&S12** for SGL and HCBA, respectively.

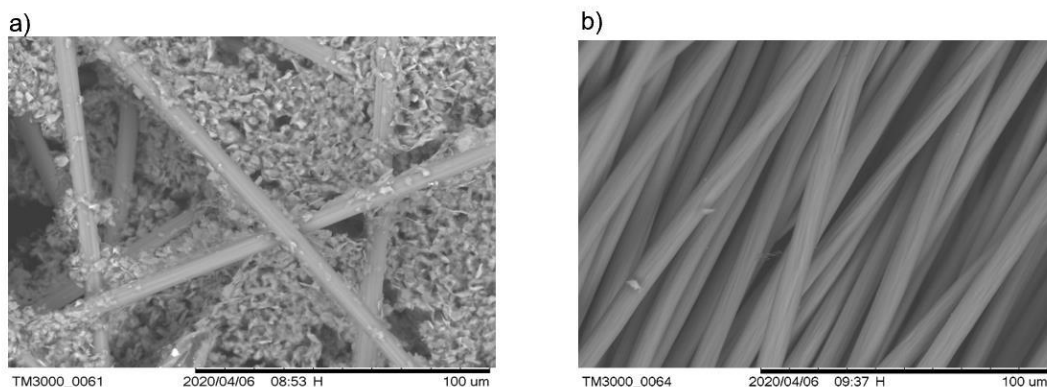


Figure S10. SEM images of (a) SGL carbon paper, and (b) HCBA cloth

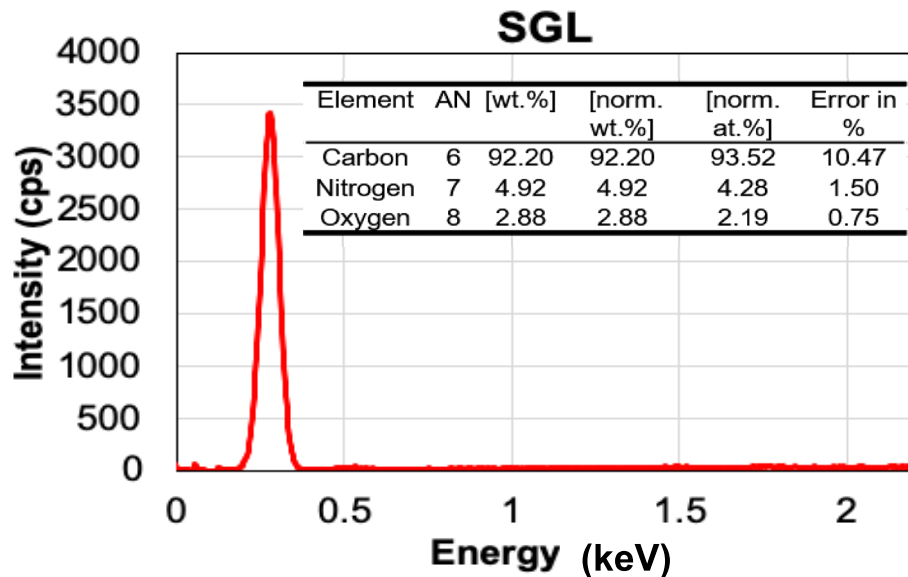


Figure S11. EDS analysis of SGL carbon paper electrode

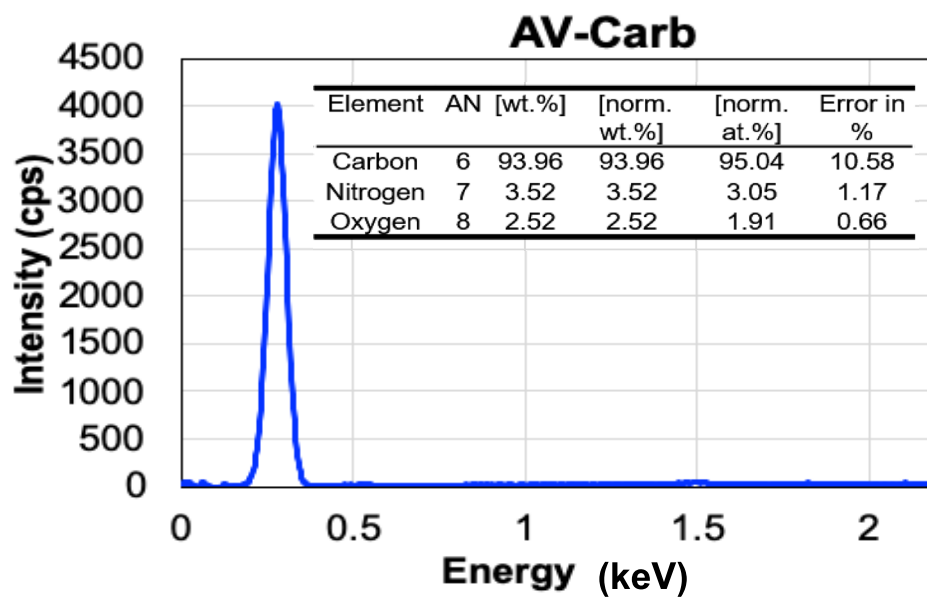


Figure S12. EDS analysis of HCBA carbon cloth electrode

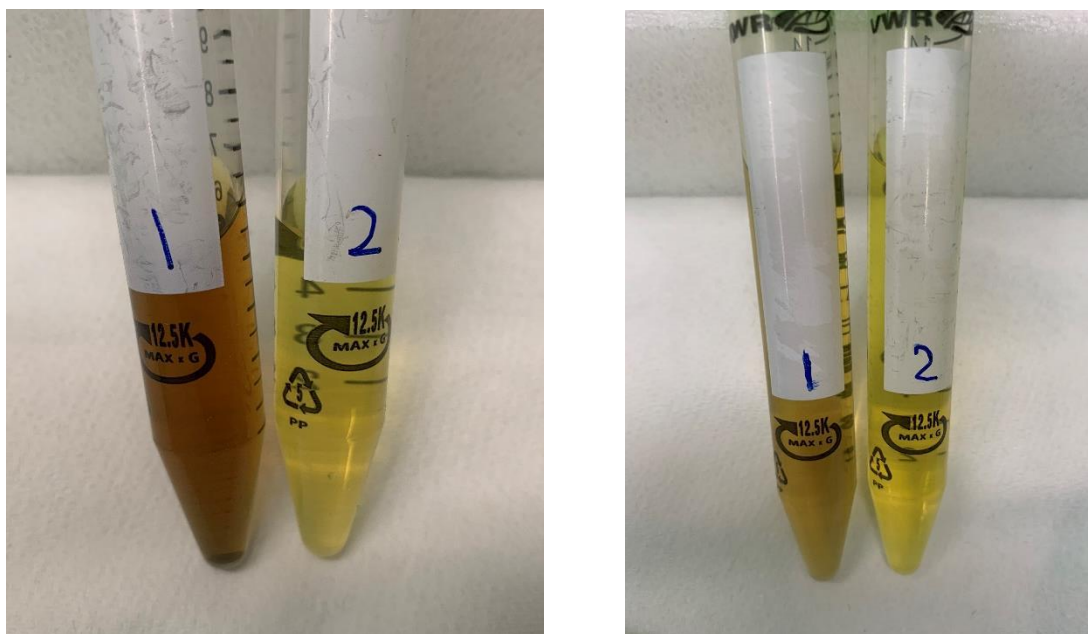


Figure S13. Cycled electrolytes for 0.1 M ferri-/0.1 M ferrocyanide pH 14 volumetrically unbalanced compositionally symmetric cells with SGL electrodes (labeled 1) or HCBA electrodes (labeled 2). CLS electrolytes are shown in the image on the left, NCLS electrolytes in the image on the right.

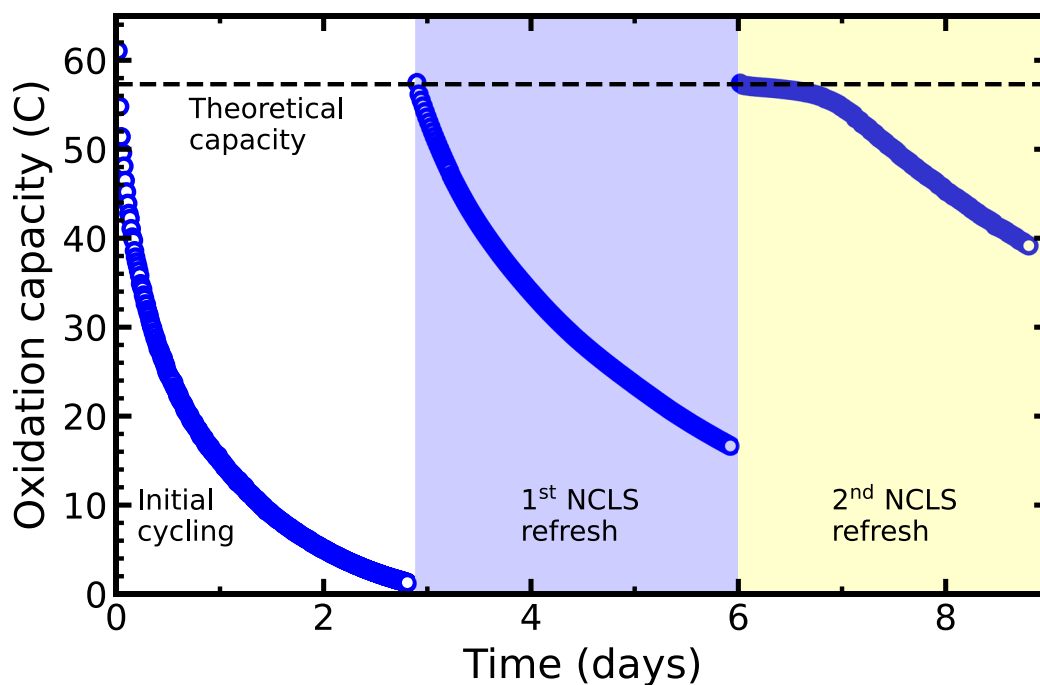


Figure S14. Potentiostatic cycling of a 0.05 M ferri-/0.05 M ferrocyanide pH 14 volumetrically unbalanced compositionally symmetric cell (6 mL CLS vs 11 mL NCLS) with SGL electrodes. The NCLS was replaced after approximately 3 days, and 6 days, with 13 mL of fresh 50% SOC electrolyte.